Development of Sheet Palletizing Manipulator Based on Multi-link Mechanism

zhihua CHEN (chen1314zh@163.com)
Beijing institute of technology https://orcid.org/0000-0003-1455-674X
Shoukun Wang
Beijing Institude of technology
Quan Liu
Beijing Information Science and Technology University
Junzheng Wang
Beijing Institude of technology

Original Article

Keywords: Multi-link controllable mechanism, Glass palletizing manipulator, Structural design, Finite element analysis, ILC

Posted Date: June 25th, 2020

DOI: https://doi.org/10.21203/rs.3.rs-36825/v1

Development of Sheet Palletizing Manipulator based on Multi-Link Mechanism

Chen Zhihua[a,b], Wang Shoukun[a,b], Liu Quan[c] ,Wang Junzheng[a,b]

[a] Key Laboratory of Intelligent Control and Decision of Complex Systems, School of Automation, Beijing Institute of Technology, Beijing 100081, China
[b] Key Laboratory of Servo Motion System Drive and Control, Ministry of Industry and Information Technology, School of Automation, Beijing Institute of Technology, Beijing 100081, China
[c] New Energy Laboratory, College of Mechanical and Electrical Engineering, Beijing Information Science and Technology University, Beijing 100192, China

Abstract: In view of the disadvantages of Traditional tandem joint type thin-plate palletizing robots using push-down adsorption sorting, such as moving path complexity, large occupied space, joint error stack and low end control precision, a novel multi-link mechanism thin-plate palletizing robot is developed. The kinematics analysis is carried out based on the analysis of the overall structure for the manipulator, a genetic algorithm based on the stroke speed ratio K, the transmission angle γ and the four-bar size is proposed to realize the optimal design of the four-link rocker arm mechanism. Secondly, a finite element based overall structure analysis method is proposed, which obtains the most affected part of the vibration process of a manipulator and performs load verification to prevent early warning and reference of faults caused by mechanical resonance. To solve the control problem of nonlinear strongly coupled dynamic systems, an iterative learning fuzzy adaptive control algorithm is proposed to achieve the smooth running of the manipulator and the high-precision tracking of the end centroid trajectory. The experimental results verify the feasibility and effectiveness of the proposed multi-link controllable thin-plate palletizing manipulator's overall structural design and iterative learning control method, which is well applied in practical engineering.

Keywords: Multi-link controllable mechanism; Glass palletizing manipulator; Structural design; Finite element analysis; ILC

1. Introduction

With the continuous improvement of human production technology, robot technology is widely used in industrial production [1-2]. Robots have gradually replaced manual production, which not only can improve production efficiency, improve production environment, reduce production costs, but also ensure the property and life security of enterprises and workers [3-4]. Therefore, industrial robots have become the focus of research at home and abroad.

Industrial thin-plate palletizing robots are widely used, mainly using joint coordinate type and Cartesian coordinate type [5]. The joint coordinate type robot body is composed of a plurality of joints. The classic six-degree-of-freedom joint type palletizing robots have been developed by companies such as ABB in Sweden and KUKA in Germany (Fig.1(a)(b)) [6]. The articulated manipulator has a large range of motion, high flexibility, and high speed [7]. However, the articulated manipulator is equipped with a servo motor and a transmission at each joint, and the mechanical end error is superimposed by the joint errors. Thus, the rigidity of the joint of the robot is low, the moment of inertia is large, and the accuracy of the end control is insufficient, which causes the squeeze to be broken. Secondly, the Cartesian robots are representative of the thin-plate palletizing robots developed by research and development companies, such as Xin song and Yaskawa Steel (Fig.1(c)(d)). The manipulator has simple structure, large movement space and strong carrying capacity, its shortcomings are low flexibility, large floor space and low practicability [8-9]. In addition, most industrial palletizing robot ends take a downward suction and grab of the sheet [10]. However, the method of downward suction requires extremely high control precision, otherwise the thin plate is easily crushed and damaged [11].

Compared with the traditional coordinate manipulator, the multi-link controllable mechanism is an important branch of our modern control mechanism [12-15]. It is a system motion mechanism consisting of multiple multi-link mechanisms. In this paper, a thin plate online palletizing manipulator based on multi-link controllable mechanism is designed (Fig.2), which has the following advantages: (1) Servo motor and linear motion driver are fixed on the base frame，which can reduce the joint inertia and joint error superposition. (2) The robot can be turned over by using crank-rocker mechanism with simple motion path, and the quick return characteristic of crank-rocker mechanism can improve the efficiency of palletizing and sorting. (3) In order to reduce the cost and reduce the breakage rate of the thin plate, an upward suction mechanism is proposed. The end manipulator is composed of parallel four-bar linkage and sucker，which is intersected between rollers. The pneumatic cylinder is used to drive the parallel four-bar, which can realize the adsorptive movement of the upper support of the end manipulator arm and avoid the extrusion damage of the thin plate due to the insufficient control accuracy.

In this paper, our main contribution of this work are as follows:

(1) In view of the disadvantages of Traditional tandem joint type thin-plate palletizing robots using push-down adsorption sorting, such as moving path complexity, large occupied space, joint error stack and low end control precision, a novel multi-link mechanism thin-plate palletizing robot is developed.

(2) In order to meet the working requirements of the TPOPM and improve production efficiency, a novel

structural parameter designing method which combines genetic parameter designing method which combines genetic algorithm method and finite element-based structural analysis method together is proposed.

(3) To solve the problem of control accuracy, an iterative learning fuzzy adaptive control algorithm is proposed to achieve the smooth running of the manipulator and the high-precision tracking of the end centroid trajectory.

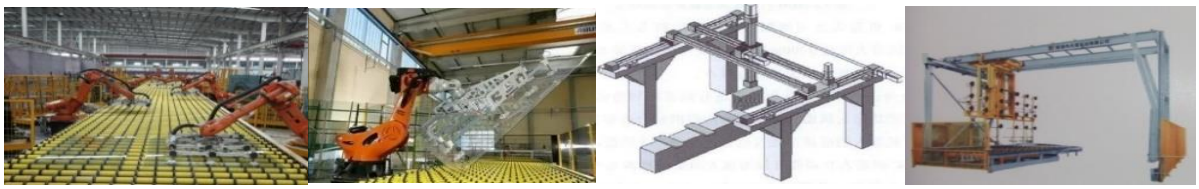

(a) (b) (c) (d)

Fig.1. Physical prototype of traditional industrial palletizing manipulator.

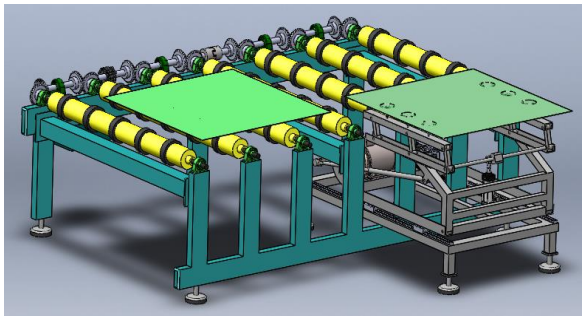

Fig.2. Three-Dimensional Model of Multi-Link Thin Plate Palletizing Robot.

The rest of this paper is organized as follows. In Section 2, the mechanical structure, kinematic analysis, and structural parameter optimization is introduced. In Section 3, the structural analysis based on finite element is proposed. It includes modal analysis, transient analysis, mechanical strength check. In Section 3, an iterative learning control strategy is designed. This Design method and control strategy are verified by experiments in Section 5. Finally, conclusions works are drawn in Section 6.

2. Palletizing robot overall design

2.1 Robot overall mechanism analysis

The new TPOPR designed in this work is mainly based on the theory of multi-degree-of-freedom controllable mechanism. The overall mechanism number setting and motion design sketch are shown in Table 1 and Fig. 3:

Table 1
Calibration of the integral rod of the palletizing robot.

Number	Name	Number	Name
1	First active rod	6	Keep parallel bars
2	First link	7	End suction arm
3	Flip rocker arm	8	Second active rod
4、5	Slider	9	Cylinder

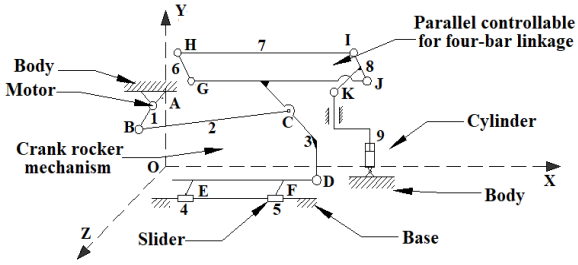

Fig.3. Schematic diagram of the palletizing robot movement.

As shown in Fig. 3, the whole body of the manipulator is mounted on the base. The servo motor, and the reducer and the base rail are installed at the bottom of the fuselage. The whole body realizes horizontal X-direction movement under the moving pairs 4 and 5. The first active rod 1 is connected to the first link 2 through the rotating

pair B. The first link 2 is connected to the flip rocker 3 through the rotating pair C. The motor A is installed at the bottom of the fuselage, and the first active rod 1(FAR 1) is driven by the motor rotating motion. Under the push of the active rod 2, the four-link rocker arm mechanism can realize the reciprocating motion.

The FAR 1, the second link 2, the flipping rocker 3, and the bottom of the fuselage constitute the first parallel controllable four-bar mechanism. The servo motor is used to drive the FAR 1 to realize the robot flipping. The parallel link 6, the end suction cup arm 7, the second active rod 8, and the top of the flip rocker 3 constitute a second parallel controllable four-bar mechanism. The second active rod 8 is pushed under the expansion and contraction of the cylinder 9 to realize the lifting movement of the end suction cup arm 7 in the Y direction. The rotating pairs G, H, I, and J form a parallelogram, ensuring that the end suction cup arm 7 and the top of the rocker arm 3 are always parallel.

2.2 DOF Analysis of Manipulator Mechanism

As shown in Fig.3, the space coordinate system X-Y-Z of the robot motion is established, and the number of moving components, planar low pairs (moving and rotating pairs), planar high pairs of the motion sketch for the palletizing robot are analyzed. The formula for calculating the degree of freedom is as follows:

$$F = 3n - \left(2P_l + P_h\right) \tag{1}$$

where, F is the degree of freedom, n is the component number, P_l is the planar low pair, P_h is the plane high pair.

According to section 2.1 and formula (1), the degree of freedom of the robot mechanism can be calculated as follows:

$$F = 3n - \left(2P_l + P_h\right) = 3*7 - \left(2*9 + 0\right) = 3$$

2.3 Kinematics analysis of four-link rocker arm module

The movement structure of the thin plate palletizing robot as shown in Fig. 4. The absolute coordinate system xyz is established for the robot base support frame, and the relative coordinate system $x_1 y_1 z_1$ is established for the robot body. The manipulator four-link rocker mechanism module is composed of a crank AB, a first link BC and a second rocker arm. The movement of the mechanical body relative to the X-axis direction of the absolute coordinate system is mainly realized by a servo motor device installed at the bottom of the fuselage. In the relative coordinate system, the crank AB is driven by the servo motor to complete the flip. The E point indicates the position of the suction arm at the end of the manipulator. Displacement, velocity, and acceleration change values at the end of the manipulator are calculated by the motion relationship between the absolute coordinate and the relative coordinate, thereby obtaining the state of movement of the manipulator.

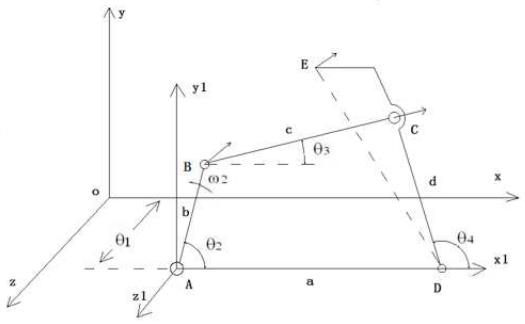

Fig.4. Schematic diagram of the thin plate palletizing robot movement.

As shown in Fig. 4, the four-link rocker arm lengths are: a, b, c, d, and the angles of the relative coordinate system level x1 axis are $\theta_1, \theta_2, \theta_3, \theta_4$. The four-bar mechanism ABCD constitutes a closed vector polygon whose vector sum is zero, and the formula can be listed according to the vector loop method:

$$\vec{b} + \vec{c} = \vec{a} + \vec{d} \tag{2}$$

In the closed quadrilateral ABCD, the angular displacement component is obtained according to the displacement vector equation (1):

$$\begin{aligned} b\cos\theta_2 + c\cos\theta_3 &= a\cos\theta_1 + d\cos\theta_4 \\ b\sin\theta_2 + c\sin\theta_3 &= a\sin\theta_1 + d\sin\theta_4 \end{aligned} \tag{3}$$

Then find the first-order reciprocal of equation (3) to get the angular velocity:

$$\begin{aligned} -\omega_2 b\sin\theta_2 - \omega_3 c\sin\theta_3 &= -\omega_1 a\sin\theta_1 - \omega_4 d\sin\theta_4 \\ \omega_2 b\cos\theta_2 + \omega_3 c\cos\theta_3 &= \omega_1 a\cos\theta_1 + \omega_4 d\cos\theta_4 \end{aligned} \tag{4}$$

when the thin plate palletizing robot is in the initial position, θ_1, θ_2,and the angular velocity ω_2 of crank AB can be obtained. Then simplify the formula (4) and use the matrix form to represent ω_3, ω_4:

$$\begin{pmatrix} -c\sin\theta_3 & d\sin\theta_4 \\ c\cos\theta_3 & d\cos\theta_4 \end{pmatrix}\begin{pmatrix} \omega_3 \\ \omega_4 \end{pmatrix} = \begin{pmatrix} \omega_2 b\sin\theta_2 \\ -\omega_2 b\cos\theta_2 \end{pmatrix} \tag{5}$$

Combining the above formulas(2-5), we can find:

$$\begin{aligned} \omega_3 &= -\omega_2 b\sin(\theta_2-\theta_4)/\left[c\sin(\theta_3-\theta_4)\right] \\ \omega_4 &= \omega_2 b\sin(\theta_2-\theta_3)/\left[d\sin(\theta_4-\theta_3)\right] \end{aligned} \tag{6}$$

Then use the formula (6) to find the first-order reciprocal, people can find the angular acceleration:

$$\begin{aligned} \alpha_3 &= \frac{-\omega_2^2 b\cos(\theta_2-\theta_4)-\omega_3^2 c\cos(\theta_3-\theta_4)+\omega_4^2 d}{d\sin(\theta_3-\theta_4)} \\ \alpha_4 &= \frac{\omega_2^2 b\cos(\theta_2-\theta_3)-\omega_4^2 d\cos(\theta_4-\theta_3)+\omega_3^2 c}{d\sin(\theta_4-\theta_3)} \end{aligned} \tag{7}$$

Combined with the rod length relationship in Fig.4, the relative velocity and absolute velocity of point E can be listed:

$$\begin{aligned} v_{E\,rs} &= l_{ED}\cdot\omega_3 = d\cdot\omega_3 \\ \vec{v}_{E\,as} &= \vec{v}_{E\,rs}+\vec{v}_{E\,is} = \vec{v}_{E\,rs}+\vec{v}_{x-axis\,rs} \end{aligned} \tag{8}$$

where, $v_{E\,rs}$ is the relative velocity, $\vec{v}_{E\,as}$ is the absolute velocity vector, $\vec{v}_{E\,rs}$ is the relative velocity vector, $\vec{v}_{E\,is}$ is the implicated velocity vector, $\vec{v}_{x-axis\,rs}$ is the relative velocity of the x-axis direction vector.

Similarly, the relative acceleration and absolute acceleration of point E can be listed:

$$\begin{aligned} a_{E\,ra} &= \vec{a}_r^{\,t}+\vec{a}_r^{\,n} = \vec{l}_{ED}\cdot\alpha_4+\vec{l}_{ED}\cdot\vec{\omega}_4^{\,2} \\ \vec{a}_{E\,aa} &= \vec{a}_{E\,ra}+\vec{a}_{E\,ia}+\vec{a}_{E\,ca} \end{aligned} \tag{9}$$

where, $a_{E\,ra}$ is the relative acceleration, $\vec{a}_r^{\,t}$ is the tangential acceleration, $\vec{a}_r^{\,n}$ is the axial acceleration, $\vec{a}_{E\,aa}$ is the absolute acceleration vector, $\vec{a}_{E\,ra}$ is the relative acceleration vector, $\vec{a}_{E\,ia}$ is the implicated acceleration vector, $\vec{a}_{E\,ca}$ is the Coriolis acceleration vector.

Since $\vec{a}_{E\,ca}$ is zero during the movement, as long as the angle ($\theta_i, i=1,2,3,4$) of the starting point of the sheet palletizing robot and the length ($l_i, i=1,2,3,4$) of each rod are given, the speed and acceleration of the end of the arm can be obtained according to the above analytical method.

2.4 Optimization design of four-link rocker arm module

According to the analysis of section 2.1, the TPOPM is mainly composed of crank rocker mechanism, parallel four-bar mechanism and base slider mechanism. Four-bar rocker mechanism (crank-rocker mechanism) includes two aspects of motion and force characteristics, which is the key device of thin plate palletizing manipulator. In addition, the quick return characteristic of crank-rocker mechanism can improve the sorting efficiency of thin plate palletizing manipulator. The kinematic and force characteristics of the mechanism need to be considered in the design:

(1) Increasing the travel speed ratio *k* of the mechanism, which can improve the quick return characteristics.

(2) The transmission angle γ is as large as possible, which can improve the transmission characteristics of the system.

(3) On the premise of meeting the actual production demand, considering the lightweight of the overall structure, the size of the mechanism should be reduced as much as possible.

Therefore, the ratio of the weighting coefficients of the stroke speed ratio *k*, the transmission angle γ, and the four-bar size in the total objective function. The total objective function is optimized by the genetic algorithm in MATLAB tool, and the optimal size of the four-link rocker arm mechanism is obtained.

2.4.1. Rocker arm motion constraint

The TPOPM rocker arm module adopts a crank rocker mechanism, as shown in Fig. 4, the four lever lengths of the crank rocker are set as: $\{a,b,c,d\}$, and as this optimization design variable, let: $x=[x_1,x_2,x_3,x_4]^T=[a,b,c,d]^T$.

(1) Link size constraint

① In Fig. 4, there is a crank lever b, and the sum of the two extreme poles is smaller than the remaining two poles:

$$\begin{cases}(a+c+d)-2\max\{a,c,d\}-b\geq 0;\\ b+c\leq a+d;\\ \min\{a,c,d\}\geq b;\end{cases} \tag{10}$$

② When designing the length of four rods, according to the actual requirements, given the range of a, b, c, d size, the design of the rod length is more reasonable:

$$\begin{cases}a_{\min}\leq a\leq a_{\max};\\ b_{\min}\leq b\leq b_{\max};\\ c_{\min}\leq c\leq c_{\max};\\ d_{\min}\leq d\leq d_{\max};\end{cases} \tag{11}$$

(2) Transmission angle constraint

According to the data, in the case of general mechanical design, $\min[\gamma]=40^0$, In some special cases, $\min[\gamma]=50^0$. The design of the connecting rod adopts $\min[\gamma]=40^0$, which is the transmission angle range:

$$\gamma_{\min}\geq[\gamma]=40^0 \tag{12}$$

2.4.2. Establish objective function and solve

In this paper, the four-bar size of the crank rocker of the TPOPR is optimized. Three sub-objective functions such as stroke speed ratio k, transmission angle γ, and four-bar size minimum are established to adjust each proportion. Using genetic algorithms to solve the optimal results. By referring to [18-19], the Three sub-objective functions are established as:

(1) The maximum objective function of the stroke speed ratio k is $F_1(x)$:

First, let: $f_1(x)=k$:

$$f_1(x)=\frac{\pi+\arccos\dfrac{b^2+c^2-2d^2\sin^2(\phi/2)}{b^2-c^2}}{\pi-\arccos\dfrac{b^2+c^2-2d^2\sin^2(\phi/2)}{b^2-c^2}} \tag{13}$$

Only when the stroke speed ratio k is greater than 1, and the crank rocker mechanism has a quick return characteristic. Set the stroke speed ratio range according to actual requirements:

$$\begin{cases}k_{\min}=\min f_1(x)=1;\\ k_{\max}=\max f_1(x)=3;\end{cases} \tag{14}$$

Establish the objective function of the stroke speed ratio as:

$$F_1(x)=\left[\frac{k_{\max}-f_1(x)}{k_{\max}-k_{\min}}\right]^{\frac{1}{2}},\left(0\le F_1(x)\le 1\right) \tag{15}$$

(2)The maximum objective function of the transmission angle $\gamma_{\min}$ is $F_2(x)$:

First, let: $f_2(x)=\gamma_{\min}$:

$$f_2(x)=\begin{cases}\gamma_1\le 90^0, f_2(x)=\gamma_1=\arccos\dfrac{c^2+d^2-(a-b)^2}{2cd}\\ \gamma_2\ge 90^0, f_2(x)=\min(\gamma_1,\pi-\gamma_2)=180^0-\arccos\dfrac{c^2+d^2-(a+b)^2}{2cd}\end{cases} \tag{16}$$

Combining the above formulas(12), the transmission angle range is:

$$\begin{cases}\gamma_{\min}=\min f_2(x)=[\gamma];\\ \gamma_{\max}=\max f_2(x)=180^0;\end{cases} \tag{17}$$

Establish the objective function of the transmission angle as:

$$F_2(x)=\left[\frac{\gamma_{\max}-f_2(x)}{\gamma_{\max}-\gamma_{\min}}\right]^{\frac{1}{2}},\left(0\le F_2(x)\le 1\right) \tag{18}$$

(3) The minimum objective function of the sum of the four bars is $F_3(x)$:

First, let:

$$f_3(x)=-(a+b+c+d) \tag{19}$$

In addition, *I* and *J* respectively indicate the structural dimensions defined by the motion pair and the installation conditions, and can be obtained:

$$\begin{aligned}m_{\min}&=\min f_3(\mathrm{x})=-4I;\\ m_{\max}&=\max f_3(\mathrm{x})=-4J;\end{aligned} \tag{20}$$

Finally, we build the objective function of the sum for the smallest dimensions:

$$F_3(x)=\left[\frac{m_{\max}-f_3(x)}{m_{\max}-m_{\min}}\right]^{\frac{1}{2}},\left(0\le F_3(x)\le 1\right) \tag{21}$$

(4) Total objective function $F(x)$

The above has established three sub-objective functions such as stroke speed ratio k, transmission angle γ, rod length and minimum. The total objective function is now established, and the proportion of the sub-objective function $f_i(x),(i=1,2,3)$ in the total objective function's weight coefficient ω_i needs to be given. And multi-objective function optimization becomes a single objective function optimization. The following is the total objective function $F(x)$:

$$F(x)=\sum_{i=1}^{n}\omega_i F_i(x),(i=1,2,3) \tag{22}$$

where, the sum of the weighting coefficients of the sub-objective functions must satisfy：

$$\begin{aligned}&\omega_i\ge 0;\\ &\sum_{i=1}^{n}\omega_i=1;\end{aligned} \tag{23}$$

In summary, considering and giving the weighting ratio of the three major transmission performance indicators, the optimization objective function of the four-link rocker arm mechanism of the palletizing manipulator is:

$$F(x)=\omega_1 F_1(x)+\omega_2 F_2(x)+\omega_3 F_3(x);$$
$$0\le F_i(x)\le 1,\quad i=1,2,3; \tag{24}$$

2.4.3. Calculation results of genetic algorithm

According to the theoretical analysis of 2.3.1-2.3.2 sections, three sub-objective functions of travel speed ratio k, transmission angle γ , four-bar size minimum are established in MATLAB. By adjusting their respective proportions under three working conditions, the optimal results are obtained by genetic algorithm.

Parameter setting steps:

(1) Need to be in the "fitness function" use @+mubiao to call the pre-written total objective function.

(2) Set the total number of target function variables in "Number of variables" to 4.

(3) Set the constraint A= [-1,1,-1,1;1,1,-1,-1;1,-1,1,1], lower[900,200,600,400], upper[1300,400,1300,900].

The results of this iteration as shown in Fig.5. and Table .2.

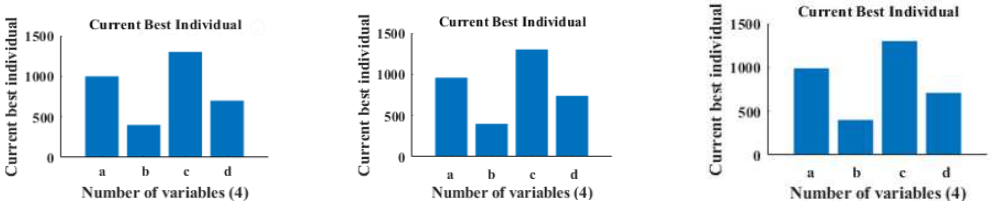

(a) Conditions 1 (b) Conditions 2 (c) Conditions 3

Fig.5. Optimized results under three working conditions.

Table 2. Optimized results under three working conditions.

Variable / Working condition	a	b	c	d	k	γ_{min}
ω_1=0.40, ω_2=0.35, ω_3=0.25	1003	396	1289	712	1.35	48.5
ω_1=0.35, ω_2=0.25, ω_3=0.40	998	384	1291	708	1.56	46.7
ω_1=0.35, ω_2=0.40, ω_3=0.25	985	376	1296	696	1.49	49.2

2.4.4. Results analysis and selection under three working conditions

According to the results of section 2.4.3, the values of $a_i,b_i,c_i,d_i,k_i\,(i=1,2,3)$ (Table.2) under three working conditions can be obtained. Then, the three models of different sizes are modeled in SolidWorks software and imported into ADAMS for simulation. The range of hinge A, B, C, D stress and transmission angle of four-bar rocker mechanism can be obtained(Fig.6-Fig.7). On the premise of meeting the design criteria of 2.4 sections ((1)The size of the mechanism should be reduced as much as possible; (2) The transmission angle γ is as large as possible; (3) Travel speed ratio k greater than 1), the minimum stress at A, B, C and D is selected as the optimal result.

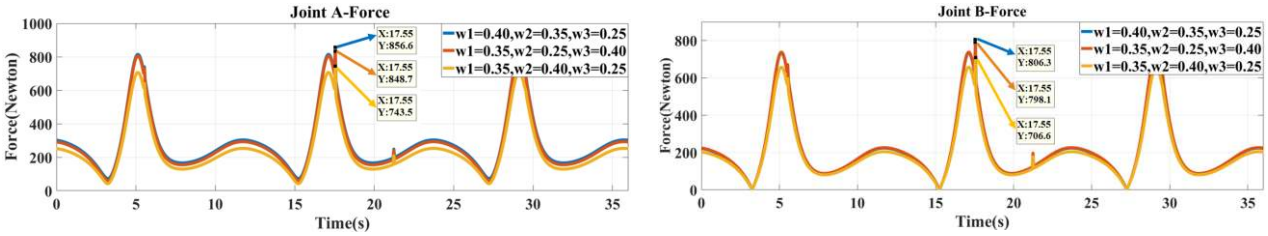

(a) Force on Joint Hinge A (b) Force on Joint Hinge B

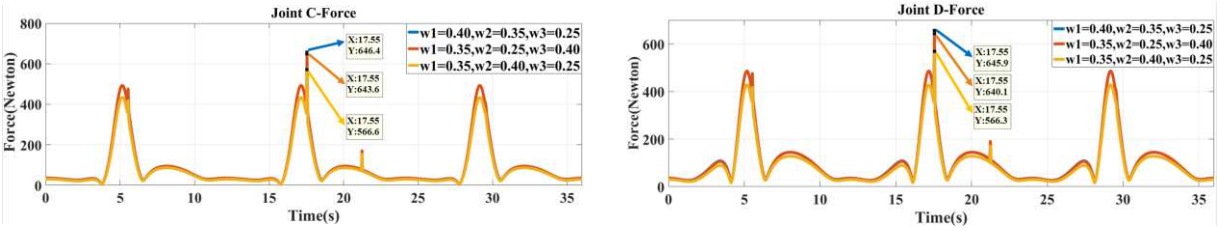

(c)Force on Joint Hinge C (d) Force on Joint Hinge D

Fig.6. Force on Joint Hinges A, B, C and D under Three Working Conditions.

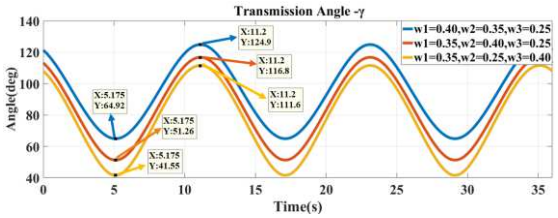

Fig.7. Transmission angle under Three Working Conditions.

The four stresses of A, B, C and D under three working conditions are shown in Fig. 6 and Table 3, the four-bar rocker arm module has the greatest force at point A under three working conditions, and the force at point A, B, C, D in case $w_1=0.40, w_2=0.35, w_3=0.25$ and $w_1=0.35, w_2=0.25, w_3=0.40$ is greater than that in case $w_1=0.35, w_2=0.40, w_3=0.25$, which raises the requirement for the stiffness of the hinge. In addition, compared with $w_1=0.40, w_2=0.35, w_3=0.25$ and $w_1=0.35, w_2=0.25, w_3=0.40$, the stress drop rate at three points of B, C, D under $w_1=0.35, w_2=0.40, w_3=0.25$ is about 12.30%, and the maximum drop rate is 13.20% at point A. Therefore, without affecting the overall performance, the structure should be designed as lightweight and miniaturized as possible. Obviously, the four-bar under B condition is more in line with the design requirements. Obviously, the four-bar under $w_1=0.35, w_2=0.40, w_3=0.25$ condition is more in line with the design requirements.

Table 3. Force on joint hinges A,B,C,D under three working conditions.

Point / Working condition	A(N)	B(N)	C(N)	D(N)
ω_1=0.40, ω_2=0.35, ω_3=0.25	856.6	806.3	646.4	645.9
ω_1=0.35, ω_2=0.25, ω_3=0.40	848.7	798.1	643.6	640.1
ω_1=0.35, ω_2=0.40, ω_3=0.25	743.5	706.6	566.6	566.3
$F_{max}-F_{min}$	113.1	99.7	79.8	79.6
$\Delta F/F_{max}(\%)$	13.20	12.36	12.34	12.32

Table 4. Transmission angle change under three working conditions.

Variable / Working condition	γ_{min}	γ range(degree)	$\gamma \geq \gamma_{min}$
ω_1=0.40, ω_2=0.35, ω_3=0.25	48.5	[64.92,124.9]	yes
ω_1=0.35, ω_2=0.25, ω_3=0.40	46.7	[41.55,111.6]	no
ω_1=0.35, ω_2=0.40, ω_3=0.25	49.2	[51.26,116.8]	yes

Table 5. Optimum design of Final result parameters.

Variable / Working condition	a	b	c	d	k	γ_{min}
ω_1=0.35, ω_2=0.40, ω_3=0.25	985	376	1296	696	1.49	49.2

As shown in Fig. 7, Table.2-Table.4, the travel speed ratio $k_i(i=1,2,3)$ of the four-link rocker module (crank rocker) satisfies $k_i \in [1,3]$ under three working conditions. In addition, the palletizing manipulator designed in this

paper belongs to the general mechanical design, which needs the transmission angle to meet $\gamma_i(i=1,2,3) \geq \gamma_{\min} = 40^0$, but the transmission angle γ_2 does not meet $\gamma_2 \geq \gamma_{\min} = 46.7^0$.

Therefore, combined with the analysis of 2.41-2.4.4 chapters, it can be seen that the selection of working condition $w_1 = 0.35, w_2 = 0.40, w_3 = 0.25$ as the design parameters of this mechanism (Table.5). Working condition 3($w_1 = 0.35, w_2 = 0.40, w_3 = 0.25$) not only meets the larger transmission ratio k ($k_3 > k_1$), but also meets the lightweight of the mechanism $(a_3+b_3+c_3+d_3 < a_1+b_1+c_1+d_1)$.

3. Structural analysis based on finite element

The modal analysis of the overall structure of the manipulator in three poses was carried out using the finite element ANSYS software. Obtain the overall natural frequency, shape distribution, and maximum displacement, prevent the external frequency from overlapping with the natural frequency of the manipulator and cause mechanical resonance, and provide early warning for mechanical resonance. Secondly, the robot body is in the operation of the sorting sheet, it will stimulate the support base bracket, and the harmonic response method is used to understand the deformation of the support frame under different excitations. Through the transient response analysis method to understand the change of each structure of the whole mechanism of the manipulator at the moment of motor starting and braking. Finally, static analysis of the viscous analysis cloud image showing the fragile components, to understand the influence of stress changes on the overall structure of the robot, and verify the mechanical structure overall stiffness and strength.

3.1 Modal analysis of three poses

3.1.1 Modal analysis theory

The principle of modal analysis is to transform the conventional linear stationary system vibration differential equation into modal coordinates. It is an independent equation described by modal coordinates and parameters in the case of decoupling of equations, so as to obtain the modal parameters of the system [20-22]. The modal parameter solution is based on the vibration theory, and it is obtained by techniques, such as stochastic process, mathematical statistics, integral transformation, and signal testing [23-25]. Under linear steady conditions, the overall structure of the palletizing robot can be discretized into a linear system with N-dimensional degrees of freedom. References [22] can be listed as differential equations that can be described as:

$$[M]\{\ddot{x}\}+[C]\{\dot{x}\}+[K]\{x\}=\{f(t)\} \tag{25}$$

where, $[M]$ is the mass matrix, $[C]$ is the damping matrix, $[K]$ is the stiffness matrix, $\{\ddot{x}\}$ is the acceleration vector, $\{\dot{x}\}$ is the velocity vector, $\{x\}$ is the displacement vector, $\{f(t)\}$ is the force vector.

In addition, during the overall modal analysis of the palletizing robot, due to the small resistance of the mechanical structure, it has little effect on the natural frequency and vibration mode of the fuselage, and can be regarded as an undamped free vibration system. The system differential equation can be defined as:

$$[M]\{\ddot{x}\}+[K]\{x\}=0 \tag{26}$$

Let the equation of the undamped free vibration be:

$$\{x\}=\{\phi\}\sin(\omega t+\varphi) \tag{27}$$

Combining the above formulas (25-26), the characteristic equation as:

$$\left|[K]-\omega^2[M]\right|=0 \tag{28}$$

The square value of each order natural frequency can be obtained by the above formula (25-28): $\omega^2=\{\omega_1^2,\omega_2^2,\cdots,\omega_n^2\}$. the i-order mode shape of the system is: $\{\phi\}=\{\phi_1,\phi_2,\cdots,\phi_i\}$.

3.1.2 Modal analysis process

As shown in Fig.8, the modal analysis process of the sheet palletizing manipulator is as follows:

(1) Save the three-dimensional entity model as. x-t file and put it into ANSYS software, and set up the material of each structure;

(2) Setting up unit type and material performance;

(3) Mesh generation of the model, setting boundary conditions, loads and modal orders;
(4) Solve the calculation and process the results.

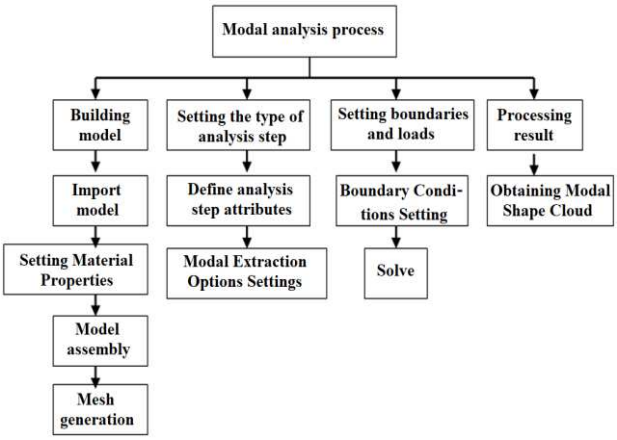

Fig.8. Modal analysis process.

3.1.3 Modal analysis results of three poses

The three pose models of the manipulator are imported into the ANSYS software. Through pre-processing, meshing, setting parameters, and finally solving, the first 6-order vibrating cloud maps, deformation quantities, and natural frequencies are obtained in the three poses as shown in Fig. 9-10 and Table 6.

The first 6-order natural frequency distribution of the manipulator pose is between 16.2 Hz and 29.4 Hz. The first-order mode vibration pattern is moved upward from the end of the manipulator arm in the Z-axis direction to the adsorption sheet, causing the right side to shake. The second and third-order mode shapes indicate the movement process of the mechanical body along the X-axis direction, and the end suction cup arms swing under the action of the thin plate load; The fourth-order mode shape indicates that the manipulator runs to the end of the X-axis, and the four-link rocker arm mechanism flips and grabs the thin plate to cause the front end of the support frame to vibrate up and down along the Z-axis. The fifth mode modal shape indicates that the end of the suction cup arm sways during the retraction of the four-link rocker arm mechanism; The sixth-order modal shape indicates that the robot is vibrating on the right side of the end suction cup due to inertia at the moment of stopping.

Similarly, the pose 2 modal analysis shows that the first six natural frequencies are distributed between 4.8 Hz and 18.2 Hz. The first-order mode shape indicates that the end suction cup arm is pitched in the Y-axis direction, and is caused by the position of the second rocker support point. The second-order mode shape indicates that the end of the suction cup arm is pressed .

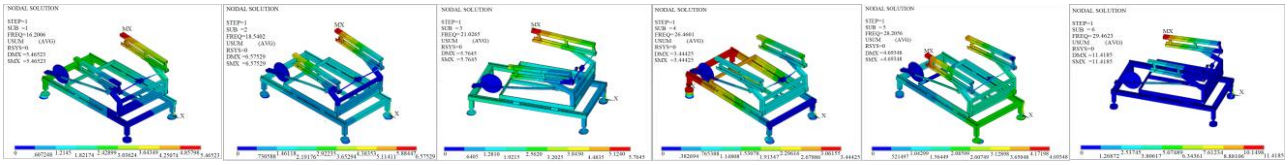

(a) Pose one.

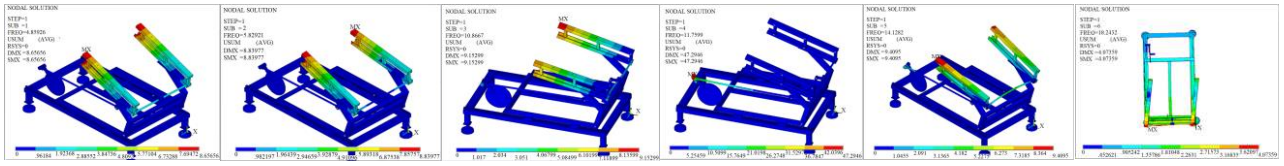

(b) Pose two.

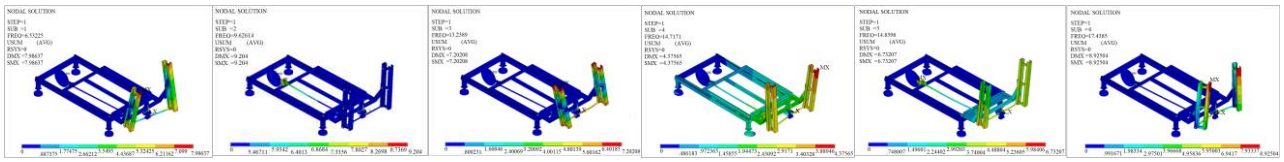

(c) Pose three.

Fig.9. The first-six vibration modes of the robot in three poses.

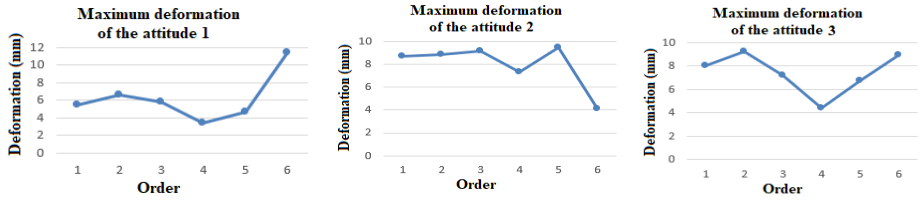

Fig.10. The first-six orders of maximum deformation under the three poses of the manipulator.

Table 6. The first-six modal parameter of the robot in three poses.

Three poses \ Order		1	2	3	4	5	6
Pose one	Natural frequency(Hz)	16.201	18.540	21.026	26.460	28.206	29.462
	Maximum deformation(mm)	5.4652	6.5753	5.7645	3.4442	4.6935	11.4185
Pose two	Natural frequency(Hz)	4.8592	5.8292	10.867	11.760	14.128	18.243
	Maximum deformation(mm)	8.6466	8.8398	9.1530	47.298	9.4095	4.0736
Pose three	Natural frequency(Hz)	6.5323	9.6261	13.239	14.717	14.840	17.438
	Maximum deformation(mm)	7.9864	9.2040	7.2021	4.3757	6.7321	8.9250

against each other along the Z-axis direction on the plane XOZ. The third-order mode shape indicates that the front end of the end suction cup arm is up and down, and the right suction cup arm is more obvious than the left side bump. The fourth-order mode shape represents the vibration of the rotating pair connected to the crank disk and the first link, where the vibration is relatively large, and the structure needs to be optimized later. The fifth-order mode shape indicates that the end suction cup is pressed in the Z-axis, and the second link is also affected by the extrusion. The sixth-order mode shape indicates that the end suction arm swings left and right in the space along the Z-axis, the vibration amplitude is relatively small and has little effect on the whole.

In the pose 3 modal analysis, the first six natural frequencies are distributed between 6.5 Hz and 17.4 Hz. The first-order mode shape indicates that the end suction cup arm swings back and forth along the X-axis direction parallel to the plane YOZ. The second-order mode indicates that the second link is connected to the crank disk by the rotating pair, and is oscillated up and down along the Y-axis. the third mode modal shape is characterized by the end suction cup arm parallel to the YOZ plane and swinging back and forth along the Z axis direction. The fourth-order mode shape indicates that the robot four-link rocker arm module and the rear half of the base vibrate up and down along the Y-axis under the action of gravity, and both ends of the end suction cup arm swing along the Z-axis. The fifth-order mode shape shows that the end suction cup arm slightly sways on the plane XOZ, which has less influence on the end suction cup arm. The sixth-order mode shape indicates that the upper portion of the end suction cup arm and the second link are pressed against each other in the Z-axis direction.

In summary, referring to the first six natural frequencies in the three poses, it is possible to avoid mechanical damage caused by overlapping with frequencies in the three poses, it is possible to avoid mechanical damage caused by overlapping with the natural frequencies and cause damage of the thin plate. In addition, the structural deformation of the first six modes is very small, and both of them are within the allowable error range, which can meet the actual production requirements.

3.2 Transient analysis of robot mechanism

3.2.1 Theory of transient response analysis

The transient response differs from the harmonic response in that the transient response calculates the vibration of the robot under transient excitation [18]. Relative to static analysis, it is necessary to calculate the response of the robot under different time history. For the palletizing robot to complete a thin-plate palletizing process, it is necessary to start and stop twice, which will impact the overall structure of the manipulator, which may cause damage to the thin plate, and may cause the mechanical structure to fall apart even under long-term operation. Therefore, transient analysis has a great significance to improve the structural life and production efficiency of the palletizing robot. According to the literature [18], the following formula can be introduced:

Harmonic response analysis follows the equation (29) kinetic equation:

$$[M]\{\ddot{x}\}+[C]\{\dot{x}\}+[K]\{x\}=\{F^c\} \tag{29}$$

where, $[M]$ is the mass matrix, $[C]$ is the damping matrix, $[K]$ is the stiffness matrix, $\{\ddot{x}\}$ is the acceleration vector, $\{\dot{x}\}$ is the velocity vector, $\{x\}$ is the displacement vector, $\{F^c\}$ is the force vector.

Transient dynamics follows the kinetic equation (29), assumption:

$$\begin{aligned}\left\{\dot{t}_{n+1}\right\}&=\left\{\dot{x}_n\right\}+\left[(1-\delta)\left\{\ddot{x}_n\right\}+\delta\left\{\dot{x}_{n+1}\right\}\right]\Delta t\\ \left\{x_{n+1}\right\}&=\left\{x_n\right\}+\left\{\dot{x}_n\right\}\Delta t+\left[\left(\frac{1}{2}-\alpha\right)\left\{\ddot{x}_n\right\}+\alpha\left\{\ddot{x}_{n+1}\right\}\right]\Delta t^2\end{aligned} \tag{30}$$

In the formula(30): α and δ is the time integral constant, Δt is the time interval, $\{x_n\}$ is the displacement vector at time t_n, $\{\dot{x}_n\}$ is the velocity vector at time t_n, $\{\ddot{x}_n\}$ is the acceleration vector at time t_n. The iterative equation can be obtained:

$$[M]\left\{\ddot{x}_{n+1}\right\}+[C]\left\{\dot{x}_{n+1}\right\}+[K]\left\{x_{n+1}\right\}=\{F\} \tag{31}$$

Inertia force：

$$\left\{F^c\right\}_e=[C]_e\left\{\dot{x}\right\}_e \tag{32}$$

where, $\left\{F^c\right\}_e$ is the damping force, $[C]_e$ is the damping matrix.

Variable stress [18]:

$$\left\{F^k\right\}_e=[K]_e\{x\}_e \tag{33}$$

where, $\left\{F^k\right\}_e$ is the variable stress experienced by the node.

3.2.2 Setting of transient response parameters

Transient response is different from modal analysis.

Table 7. Parameter Setting for Transient Response Analysis.

Variable \ Axis	X	Y	Z
Force(N)	319.5	345	267
Phase angle(^{0})	0	0	0
Frequency(Hz)	50	50	50

Transient response refers to the vibration of the palletizing manipulator under instantaneous excitation. It is necessary to calculate the response of the manipulator under different time histories. The TPOPR studied in this paper has the greatest impact on the structure of the manipulator at the moment when the motor stops and starts, which is easy to cause the thin plate damage. Therefore, it is necessary to carry out transient analysis of the base bracket and overall rack of the manipulator. The motor parameters(Table.7) are as follows: frequency 50Hz, time interval 0.001s, total step time 5s, time step 5000, XYZ three-axis force is 319.5N, 345N, 267N.

3.2.3 Analysis of the results for transient response

Through the above calculation results of the palletizing robot base support frame and the overall rack transient response, it can be concluded:

First, as shown in the left side of Fig. 11(a-b) and Table.8, the maximum total deformation is 6.5742*10^{-5}m from the transient deformation total deformation cloud map(Fig11(a)) and the stress change cloud diagram(Fig11(b)) of the base support frame, and the maximum total deformation occurs at the front part of the beam in the Z-axis direction of the manipulator. In addition, along the X axis, the end part of the beam also appears a certain deformation, and it becomes smaller in the positive direction of the X-axis, and the deformation range is between 1.4609*10^{-5}m-5.8437*10^{-5}m. The maximum stress of the support frame occurs at the bottom end of the support frame, and the maximum stress value is 0.042MPa, and the stress at other parts is very small. Therefore, the analysis shows that the base support frame can meet the requirements under the transient excitation.

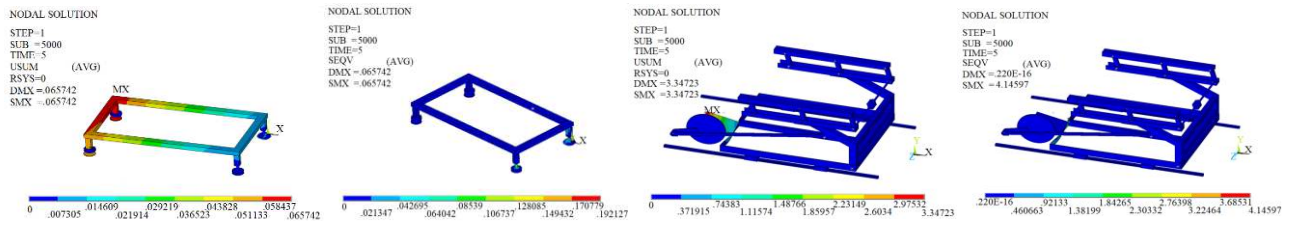

(a) (b) (c) (d)

Fig.11. Transient deformation cloud diagram and stress cloud diagram of base support frame and overall rack.

Table 8. List of parameters for transient response results.

Name \ Variable	Max-Deflection(mm)	Min-Deflection(mm)	Deflection range(mm)	Max-stress(MPa)	Min-stress(MPa)	Stress range(MPa)

Support frame	0.065742	0.007305	[0.007305,0.065742]	0.042	0.021347	[0.021347,0.042]
Overall rack	3.3472	0.371915	[0.371915,3.3472]	4.145	0.0220E-16	[0.0220E-16,4.145]

Similarly, as shown on the right side of Fig. 11(c-d)and Table.8, the maximum total deformation of the whole frame of the manipulator is 3.3472*10-3m through the overall frame transient response total deformation cloud image and the stress variation cloud image, and the maximum total deformation occurs in the robot crank motor mounting plate and the bottom of the frame, especially at the mounting plate near the outside of the motor, the deformation is the largest, from the outside to the inside, the deformation range is between $0.3719*10^{-3}$m-$3.3472*10^{-3}$m. While the other parts are small and almost negligible. In addition, the maximum stress occurs at the joint between the crank motor mounting plate and the bottom of the frame, and the maximum stress value is 4.14597 MPa. The stresses of other large parts are relatively small, basically concentrated between 0.46063MPa and 0.92133MPa, which has no effect on the overall structure.

According to the above dynamic analysis, it can be seen that the four beams of the base support frame are easily deformed, and it is easier to shake in both X and Y directions. Although the deformation amount and the shaking condition have no great influence on the overall structure of the manipulator, in order to strengthen the overall structure of the mechanism performance, you can add "ribs" to the four beams of the base support frame, and the motor control in the latter two directions needs to be improved to improve the stability of the system and reduce the glass breakage rate.

3.3 Mechanical strength check

3.3.1 Static check of sucker arm

The suction cup arms on both sides of the end of the robot are respectively equipped with three suction cups, and the thin plate is flipped under the suction of the suction arm. Thin glass was used as the experimental object, and the maximum weight of single glass was 3Kg. In addition, there are six suckers in the sucker arm, each 8N. Therefore, the sucker arm bears 38.7N on one side. Static analysis results and parameter settings are shown in Fig.12 and Table.9.

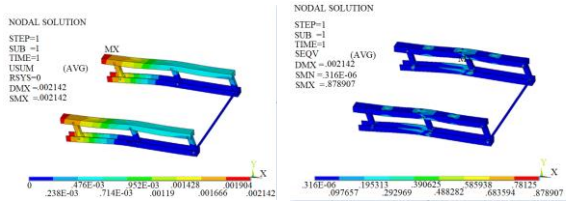

Fig.12. Static analysis cloud diagram of sucker arm

Table 9. Parameter Setting and results for Transient static.

Variable / Name	Yield strength	Left-loading	Right-loading	Max-stress
Sucker arm	206(GPa)	38.7(N)	38.7(N)	0.8789(GPa)

Under the load of the suction cup arm, the maximum deformation is $2.142*10^{-6}$mm, and the deformation is almost negligible. In addition, the material of the robot base support frame is carbon steel Q235, and its yield strength is 206GPa, while the stress cloud shows a maximum stress of 0.8789MPa, which is much smaller than the allowable stress value and appears at the joint of the rotating pair. Therefore, the check of the suction cup arm meets the design requirements.

3.3.2 Static check of the crank rocker arm

The upper end of the four-link rocker arm mechanism is equipped with a suction cup arm, and the suction cup arm is parallel to the horizontal X-axis, and the glass palletizing is completed under the turning mechanism. The weight of the upper suction cup arm of the four-link rocker arm mechanism is 30Kg, and the weight of each side of the four-link rocker arm mechanism is 147N. Static analysis results and parameter settings are shown in Fig.13 and Table.10.

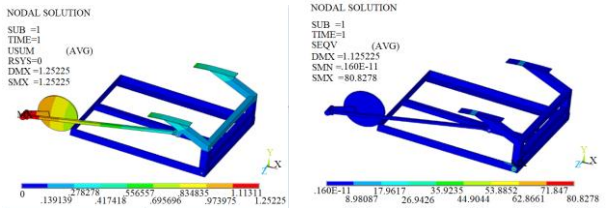

Fig.13. Static analysis cloud diagram of the crank rocker arm

Table 10. Parameter Setting for Transient static of the crank rocker arm.

Variable / Name	Yield strength	Left-loading	Right-loading	Max-stress
Crank rocker arm	206(GPa)	147(N)	147(N)	80.83(MPa)

Under the suction arm and glass load, the maximum deformation of the four-link rocker arm mechanism is $1.25226*10^{-3}$m, and the deformation position is at the crank and connecting rod rotation pair. The deformation is within the error range, and the overall position accuracy is not have a big impact. In addition, the material of the four-link rocker arm mechanism of the manipulator is carbon steel Q235, and its yield strength is 206GPa, which is much larger than the maximum stress shown by our stress cloud diagram of 80.8278MPa. Therefore, the stiffness of the material of the mechanism meets the design requirements.

4. Iterative learning control strategy

Traditional industrial robots often need to perform repetitive actions in industrial production, such as welding, spraying, assembly, handling and other repetitive industrial robots [26]. The iterative learning control method is very suitable for controlled objects with repetitive motion properties, it does not require systematic mathematical models, It uses multiple iterative corrections to control nonlinear highly coupled dynamic systems with high uncertainty, and tracking the given desired trajectory with high precision. Therefore, the iterative learning control algorithm is very suitable for the thin-plate palletizing manipulator of multi-link controllable mechanism.

Classical iterative learning control is essentially a feedforward control technique, but the convergence speed is slow. In order to improve the robustness and convergence speed of the system, the iterative learning control method with feedforward and feedback parallel configuration is used to construct the learning law, which can enhance the system robustness and improve the convergence speed compared with the traditional feedforward iterative learning control.

Feedforward-feedback iterative learning control is mainly composed of two parts, as shown in formula [34]:

$$u_i = u_i^f + u_i^q; i = (0,1,2,.....,k+1) \tag{34}$$

where, u_i^f is the feedback output signal calculated by the feedback controller of the current error value, u_i^q is the feedforward control signal generated by the iterative learning control (ILC) of the current error.

In the feedforward-feedback iterative learning control strategy, the feedforward control signal is mainly composed of two different components, which can be divided into the following two feedforward control algorithms:

$$u_i^q = u_{i-1}^q + He_{i-1}; i = (1,2,.....,k+1) \tag{35}$$

$$u_i^q = u_{i-1} + He_{i-1}; i = (1,2,.....,k+1) \tag{36}$$

Here in the above formula (35-36) are PD type iterative learning control adaptive algorithm. The algorithm (35) consists only of the feedforward control signal u_{i-1}^q. The algorithm (36) is mainly composed of the feedback signal u_{i-1}^f and the feedforward signal u_{i-1}^q, the addition of the feedback signal not only enhances the robustness of the system, but also does not affect the convergence of the feedforward system. Therefore, the feedforward-feedback iterative learning control strategy of this paper uses algorithm (36), and its control block diagram is shown in Fig. 14.

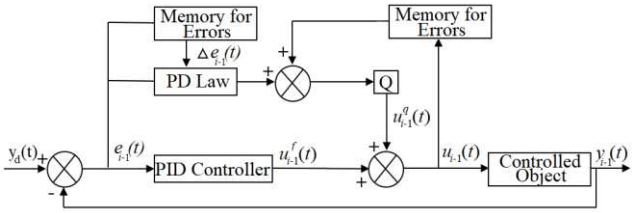

Fig.14. Feedforward-feedback iterative learning control block diagram.

As shown in Fig. 14 . $y_d(t)$ is the expected value, $e_{i-1}(t)$ is the tracking error, u_{i-1} is the control signal. The memory unit is mainly used to store the error and control signals after each iteration. Q mainly used to filter noise and interference in high frequency bands. Here, the Butterworth filter is used. The formula is as follows [27]:

$$\|Q(s)\| = \begin{cases} 1, \varpi \in [0, \varpi_c] \\ 0, \varpi > \varpi_c \end{cases} \tag{37}$$

In addition, the traditional PD type iterative learning control algorithm formula is as follows:

$$u_{i-1}^q(t) = u_{i-1}(t) + K_P e_{i-1}(t) + K_D \dot{e}_{i-1}(t) \tag{38}$$

Based on the traditional PD-type iterative learning control algorithm, an improved PD-type iterative learning control

algorithm is proposed. Under the two-dimensional fuzzy inference rule, calculating the current error $e_{i-1}(t)$ and the error variation $\Delta e_{i-1}(t)$ can change the value of K_D online. Suppose the fuzzy rules defining $e_{i-1}(t)$ and $\Delta e_{i-1}(t)$ are: { NB, NM, NS, Z, PS, PM, PB }, and according to the Mickwyck-William matrix and engineering experience, the K_D fuzzy rules are established as shown in Table.11.

Table 11. K_D Fuzzy Control Rule Table.

$\Delta e_{i-1}(t)$	$e_{i-1}(t)$						
	NB	NM	NS	Z	PS	PM	PB
NB	PB	PB	PB	PM	PM	Z	NS
NM	PB	PB	PM	PM	PS	Z	NS
NS	PB	PM	PS	PS	Z	NS	NM
Z	PM	PS	PS	Z	NS	NM	NM
PS	PM	PS	Z	NS	NM	NM	NB
PM	PS	Z	NS	NS	NM	NB	NB
PB	Z	Z	NM	NM	NM	NB	NB

In addition, it is assumed that the feedback controller in the system of Fig. 14 is represented by the symbol P, the improved PD type iterative learning control rate is represented by L, and the control object is represented by O. In order for $e_i(t)$ to converge to the equilibrium point, the convergence radius must satisfy the following formula:

$$\rho_{ILC}=\left\|\frac{Q(1-O*L)}{1+O*P}\right\|_{\infty}<1 \tag{39}$$

According to the formula (34-38) and the flow of Fig.14, the feedforward-feedback iterative learning control input signal u_i and the tracking error $e_i(t)$ formula can be listed as:

$$u_i(t)=\frac{Q(1-O*L)}{1+O*P}u_{i-1}(t)+\frac{Q*L+P}{1+O*P}y_d \tag{40}$$

$$e_i(t)=\frac{Q(1-OL)}{1+OP}e_{i-1}(t)+\frac{Q(2OL-1)-1}{1+OP}y_d \tag{41}$$

If the following inequality is satisfied for any coefficient i:

$$\left\|e_{i+1}-e_i\right\|_{\infty}\le\left\|e_i-e_{i-1}\right\|_{\infty},i=(1,2,3,.....,k+1) \tag{42}$$

Then the formula (39) is established, at which point $e_i(t)$ will converge to the equilibrium point.

In summary, the iterative learning convergence mainly depends on the control rate L and the controller P. The integral and differential links are added in the feedback controller to adjust the steady-state error of the system, and the iterative learning control method with feedforward and feedback parallel configuration is used to construct the learning law, which can enhance the system robustness and improve the convergence speed compared with the traditional feedforward iterative learning control.

5. Experiment verification

5.1 Experimental Platform and requirements

Fig.15 is a test system for the thin-plate palletizing robot experimental platform designed. The whole test device consists of multiple system devices, the experimental object is ultra-thin glass. In order to ensure the safety of the circuit during the operation for the palletizing robot, the main switch of the power supply and the main switch of the electric control cabinet adopt automatic trip switch. When the system is faulty, the circuit can be cut off to avoid damage to the system components. In addition, you need to pay attention to the following points before the experiment:

(1) The displacement sensor is installed on the right side of the end of the manipulator.

(2) The Z-axis direction is fixed, and the manipulator does not move in the Z-axis direction.

(3) Safety inspection of electrical circuits, components, and palletizing robots before the experiment.

(4) The palletizer robot X, Y, Z axis for origin search to ensure that it is in the initial position.

(5) Airtight inspection of the air source unit and the vacuum generator unit to ensure good air tightness.

(6) Switch the palletizing robot control system to automatic operation to avoid intermittent operation.

(7) Checking the end arm displacement sensor and terminal connection are accurate, to ensure the validity of the collected data.

In addition, in order to verify the feasibility of the structure and control method design of the palletizing manipulator in this paper, the PD-type iterative learning control algorithm proposed in this paper is compared with the classical PID control

algorithm. During the experiment, the displacement sensor is installed on the right side of the end of the manipulator, and the displacement sensor is used to measure and track the displacement change of X, Y, Z axis, and the displacement change of X, Y, Z axis is fitted to the space trajectory.

5.2 Experimental test and result analysis

Under the condition that all control parameters of the experimental platform are the same, the position tracking tests of PD-ILC and traditional PID control algorithm are carried out, and their control effects are compared and analyzed. Fig.16 and Fig.17 respectively plot the position change and tracking error curves of the traditional PID control algorithm and the Iterative 20th in the direction of X and Y axes PD-ILC control algorithm, where Fig.16(a) the position tracking curve and Fig.16(b) the tracking error curve. As shown in Fig. 16 (a) (b),the position control result of traditional PID for X-axis direction is not ideal, the maximum tracking error is 2.40 mm and the degree of asymmetry is 15.8%, but, the control effect of PD-type ILC is better, the maximum tracking error is 1.20 mm and the degree of asymmetry is 15%. In addition, as shown in Fig. 17 (a) (b), the position control results of the Y-axis are not satisfactory with the maximum tracking error of 2.08 mm and the degree of asymmetry of 63.94%, but, the control effect of PD-type ILC is better, with the maximum tracking error of 1.42 mm and the degree of asymmetry of 57.2%. Table.13 shows the detailed data of traditional PID control and PD-ILC under the 20th iteration number, where $e^{+}_{\max}$ and $e^{-}_{\max}$ are the maximum errors of positive and negative motion of X and Y axes, K_a are asymmetry, and K are iteration times.

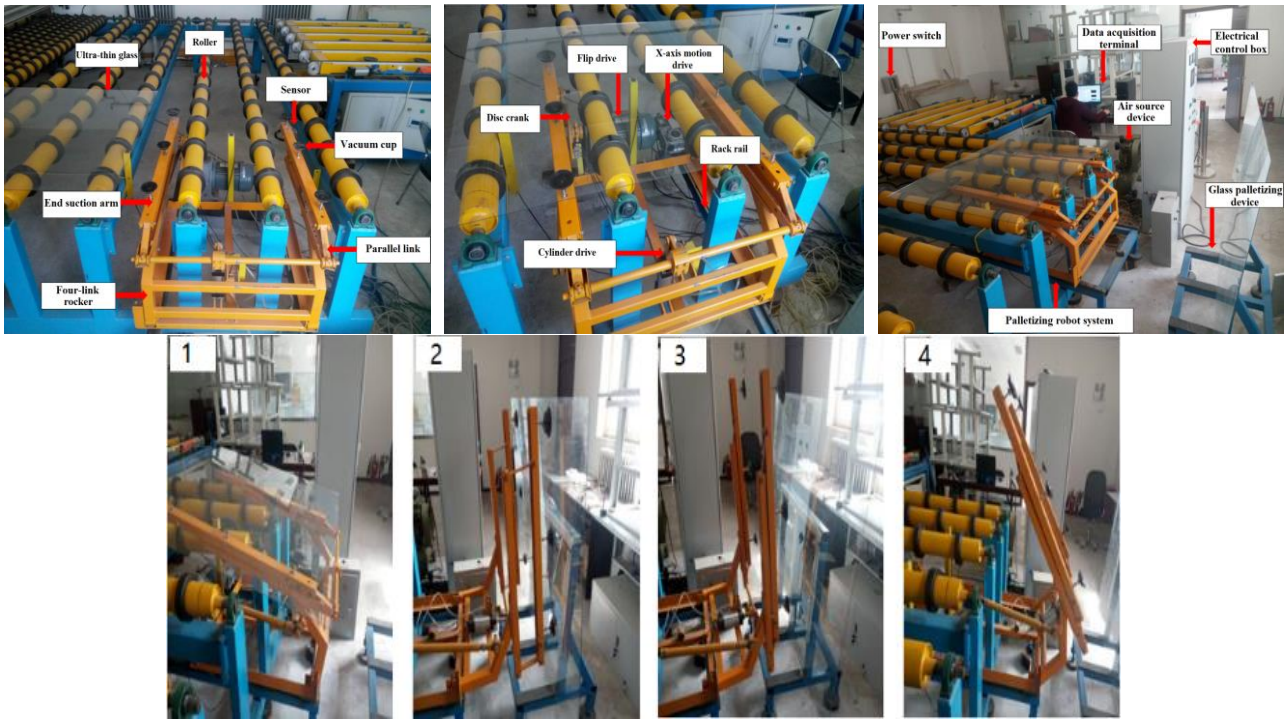

Fig. 15 Glass palletizing robot test experiment with multi-link mechanism.

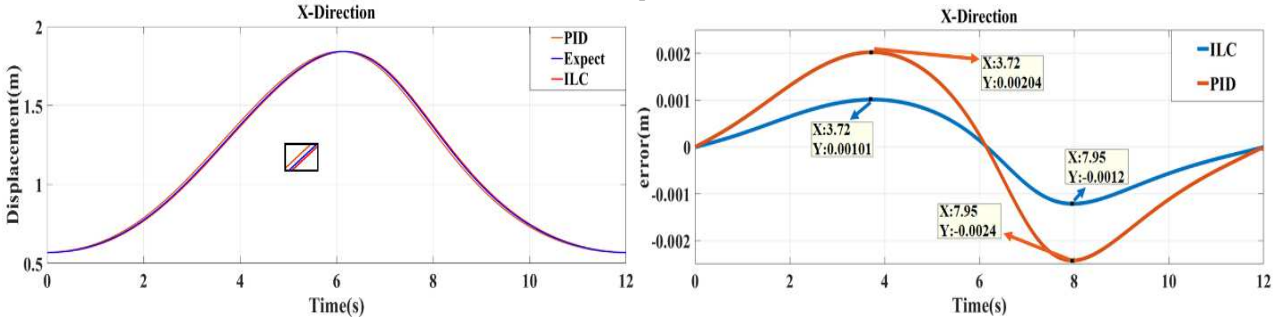

(a) X axis position tracking curve (b) X axis position tracking error curve

Figure.16 X axis test data of PID and PD-type ILC in 20th iteration.

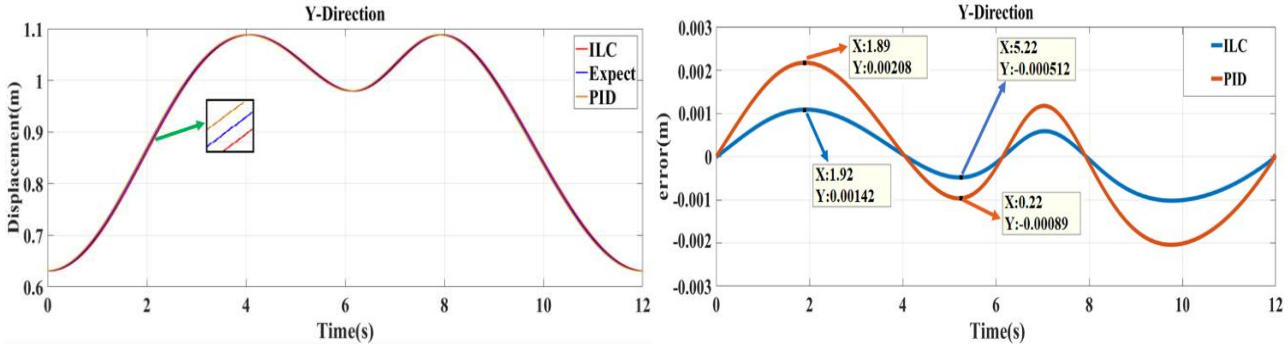

(a) Y axis position tracking curve (b) Y axis position tracking error curve

Figure.17 Y axis test data of PID and PD-type ILC in 20th iteration.

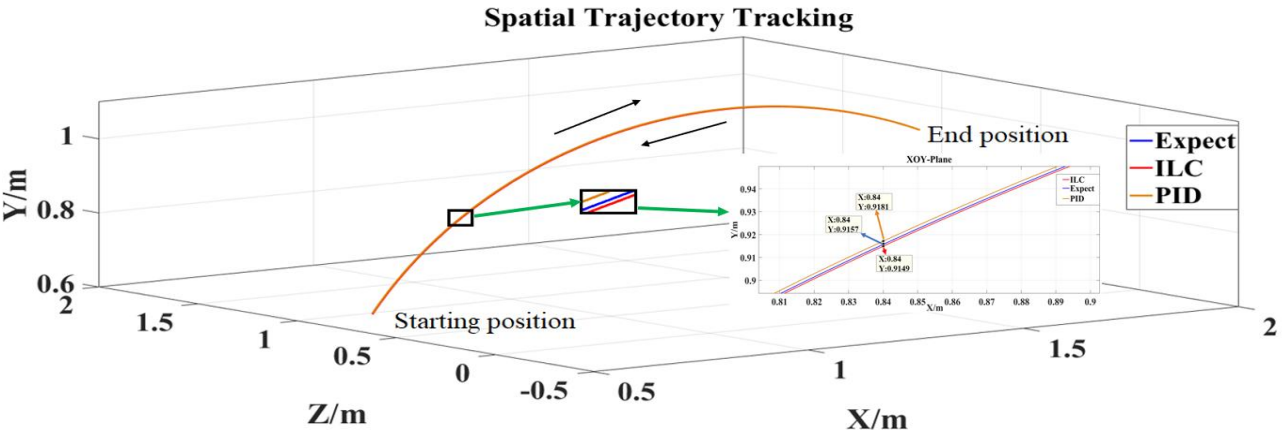

Figure.18 Three-dimensional trajectory tracking test data of PID and PD-type ILC in 20th iteration.

Table 13. Test data of PID and PD-type ILC in 20th iteration.

	Axis	X	Y	Z
e^{+}_{max} /m	PID	0.00204	0.00208	0
	PD-type ILC(K=20)	0.00101	0.00142	0
e^{-}_{max} /m	PID	0.00240	0.00089	0
	PD-type ILC(K=20)	0.00120	0.000512	0
$K_a=\frac{Abs(e^{+}-e^{-})}{Max(e^{+},e^{-})}\times 100\%$	PID	15.8	63.94	0
	PD-type ILC(K=20)	15	57.2	0

Since the multi-link thin plate palletizing manipulator is moving in three-dimensional workspace, in order to understand the end trajectory of the manipulator more intuitively, the X-Y-Z three-axis trajectory is fitted, and the control effect of the traditional PID and iterative 20th PD ILC is compared by shown in Fig.18(because the Z-axis position is fixed and unchanged, the XOZ plane and YOZ plane motion curves are not given). As shown in Fig.18, on the X-O-Y plane, the maximum tracking error of traditional PID control is 2.4 mm, but, the PD-ILC after 10 iterations is only 0.8 mm, which improves the control accuracy by 33.3%.

6. Conclusion

In this paper, a new type of palletizing manipulator is designed and relevant experiments are carried out. The conclusion is as follows:

(1) This paper designs a stacking manipulator based on crank rocker mechanism and four-bar mechanism. The servo motor and the driver are fixed on the base frame, and the flexible output of the mechanical end is realized by controlling the angle of the crank, which avoids the insufficiency of the serial robot joint caused by the installation of the servo motor and the transmission device. In addition, the suction arm at the end of the manipulator uses the way of upward lifting to sort the glass. Compared with the traditional down pressure adsorption method, the control is simple, which solves the problem of ultra-thin glass breaking caused by the low down pressure control accuracy at the end of the manipulator and reduces the glass breaking rate.

(2) The kinematics analysis of the manipulator is carried out by analytic geometry method and vector loop method. The

genetic algorithm based on the stroke speed ratio k, transmission angle γ and four-bar size is proposed to realize the optimal design of the four-link rocker arm mechanism. The feasibility and effectiveness of the design method are verified by experiment.

(3) Combined with the vibration characteristics of the glass palletizing manipulator and the ability to resist vibration, a finite element-based overall structural analysis method is proposed. The load verification of the weak link is carried out to verify the rationality of the structural design and provide early warning and reference for the faults in the later vibration.

(4) Traditional PID control is difficult to achieve ideal results for the control of strong coupling nonlinear dynamic systems. In order to improve the motion accuracy of the new multi-link palletizing robot, a PD-type ILC control method is proposed. The validity and effectiveness of the control method are verified by the experiment of thin plate online palletizing manipulator. Theoretical analysis and experimental results show that this PD-type ILC control method related to PID control can achieve thin plate online palletizing manipulator motion accuracy without establishing mathematical model or obtaining accurate loading condition

References

[1] Wang T M, Tao Y. Research status and industrialization development strategy of Chinese industrial robot. Journal of Mechanical Engineering 2014;50 (9):01-03.

[2] Brogardh T. Present and future robot control development-An industrial perspective. Annual Reviews in Control 2007;31:69-79, .

[3] Ribeiro T, Garcia I, Pereira D, Ribeiro J, Lopes G, Ribeiro A F. Development of a prototype robot for transportation within industrial environments. 2017 IEEE International Conference on Autonomous Robot Systems and Competitions (ICARSC) 2017;192-197.

[4] Qu D K. Development Situation and Prospects of Chinese Robot Industry. Bulletin of the Chinese Academy of Sciences 2015;30(3):342-346.

[5] Ji S M, Huang X H. Review of development and application of industrial robot technology. Journal of Mechanical & Electrical Engineering 2015;01:01-05.

[6] Matsushima, T. Development of vertical articulated palletizing robot． Robot 1993; (92):47-53.

[7] Liu F C, Yao B Z, Liu L M. Development and Application of High-Speed Transfer Robots Industry. Light Industry Machinery 2012;30(02):108-112.

[8] Kodaira N. High performance palletizing robot and palletizing/depalletizing system. Robot Tokyo 1994;98: 60-66.

[9] Tan M, Wang S. Research Progress on Robotics. Acta Automatica Sinica 2013;39(7): 963-965.

[10] Gao F. Reflection on the current status and development strategy of mechanism research. Journal of Mechanical Engineering 2005;41(8): 03-17.

[11] Zou H J, Lan Z H, Wang S G, Guo W Z. Research situation development trends and application prospects of mechanism theory. Journal of Mechanical Engineering 1999;35(05): 01-04.

[12] Dubowsky S et al. Dynamic Modeling of Flexible Spatial Machine Systems with Clearance Connections. Trans. ASME, J. Mech. Transmiss. Automat. Des 1987;109:87-94.

[13] Funabashi H, Ogawa K, Horie Metal. A dynamic analysis of the plane crank-and-rocker mechanisms with clearances. Bulletin of JSME 1980;23(177):446-452.

[14] Yu X W, Zhao Y, Tomizuka, Masayoshi. Automatic glass pick and place by industrial robot. ASME 2016 Dynamic Systems and Control Conference 2016;02:76.

[15] Otsuka K, Kubota H. Application of robot in the glass industry. Robot 1995;104:64-69.

[16] Li Y Y, You M. Optimization design of crank rocker structure under the given output angle constraint. Manufacturing Automation 2016;38(01):102-104.

[17] Sun Y, Zhan H Y. Optimal design of planar crank rocker mechanism according to minimum transmission angle maximum and minimum size. Mechanical design 1996;09:32-40.

[18] Su H. Research on Crank Rocker Mechanism Design. North China Electric Power University 2011;06.

[19] Tang Y H, Liu Z W, He B. Optimization design for crank-rocker mechanism based on genetic algorithm. Proceedings of the 2012 Second International Conference on Intelligent System Design and Engineering Application (ISDEA) 2012;02:417-420.

[20] Tian M Z, He F, Wang D D. Modal analysis of palletizing robot based on finite element method. Machine Tool & Hydraulics 2015;(09):80-83.

[21] Zhang W C, Chen J, Pei B H, Ma B B, Du X B. Stress analysis and modal analysis of robot manipulator. Applied Mechanics and Materials 2011;(06):75-78.

[22] Chacko, S. Dynamic analysis of compliant robotic manipulator using finite element method. International Conference on Numerical Analysis and Applied Mathematics 2005:748-752.

[23] Zhang C P, Yu F, Duan H G, Chen Y. Dynamic modeling and finite element structural optimization of glass handling robot. International Journal of Structural Integrity 2017;8(3):423-434.

[24] Lu P, Cheng D L, Shi G, Zhou Z H, Li N K. Motion Simulation and Finite Element Analysis of the Manipulator Based on SolidWorks. Applied Mechanics and Materials 2014;(07):640-645.

[25] Chen X B, Xiong C H, Xiong Y L. Kinematics Modeling and Simulation of a Passive Fourbar Linkage. Proceedings of the 2009 IEEE International Conference on Mechatronics and Automation 2009;(05):4139-4144.

[26] Wang S K, Wang J Z, Zhao J B. Application of PD-type Iterative Learning Control in Hydraulically Driven 6-DOF Parallel Manipulator[J]. Transactions of the Institute of Measurement and Control 2013:683-691.

[27] Yu S J. Study on Robust Iterative Learning Control for the Electro-Hydraulic Force Servo System. Taiyuan University of Technology 2012;05.

Declarations

Competing interests

The authors declare that we have no known competing financial interests or personal relationships that could have appeared to influence the work reported in this paper. Thank you very much for your time and consideration. Thank you sincerely! If you need anything, please send it to chen1314zh@163.com and I will reply to you in time.

Funding

This study was supported by Nation Natural Science Foundation of China under Grant 61773060.

Authors' contributions

QL was in charge of the whole trial.; ZC contributed the central idea, analysed most of the data and wrote the initial draft of the paper. SW and JW contributed to refining the ideas, carrying out additional analyses and finalizing this paper. All authors read and approved the final manuscript.

Acknowledgements

First of all, I would like to give my tutors Professor Wang Shoukun and Professor Liu Quan, who provide me with valuable ideas and experimental platform in all stages of thesis writing. Secondly, I would like to thank Professor Wang Junzheng of the laboratory for his guidance and help. Finally, I would like to thank my beloved family for their care and trust in me.

Authors' information

Zhihua Chen received the M.S. degree in Mechatronics Engineering from Beijing Information Science and Technology University. He is currently a Ph.D. student at School of Automation, Beijing Institute of Technology, China. His research interests are robot motion control, adaptive robust control.

Shoukun Wang received the B.S., M.S., and Ph.D. degree in department of automation, from Beijing Institute of Technology, Beijing, China, in 1999, 2002, 2004 respectively. He has entered in Department of Electronics and Computer Engineering, the Purdue University, West Lafayette, USA as a visiting scholar. He has been teaching at the School of Automation, Beijing Institute of Technology, since 2004. His research interests include sensor, measurement, and electro-hydraulic control. He has participated in over 30 scientific research projects since 2001, which mainly belong to measurement and servo control. He has also served as the leader in some of these works. His main work focused on Electrical-hydraulic control algorithm, robot locomotion control, and visual servoing.

Quan Liu received the Ph.D. degree from the Beijing Institute of Technology, Beijing, China, in 2004. He is the Deputy Director of the Laboratory of New energy, Beijing Information Science and Technology, where he is a Professor and Ph.D. Supervisor. His current research interests include robot technology, production line automation equipment and New energy technology (wind power, solar energy). Prof. Liu is a Member of the Subcommittee of Power Machinery Engineering of China Machinery Industry Education Association, and National New Energy Science and Engineering Professional Alliance, expert of high-end expert think tank of power industry, expert consultant of Energy Investment Committee of China Investment Association, and member of China Renewable Energy Society.

Junzheng Wang received the Ph.D. degree from the Beijing Institute of Technology, Beijing, China, in 1994. He is the Dean of the School of Automation and the Deputy Director of the Key Laboratory of Intelligent Control and Decision of Complex Systems, Beijing Institute of Technology, where he is a Professor and Ph.D. Supervisor. His current research interests include motion control, static and dynamic performance testing of electric and electric hydraulic servo system and dynamic target detection and tracking based on image technology. Prof. Wang is a Senior Member of the Chinese Mechanical Engineering Society and the Chinese Society for Measurement. He was the recipient of the Second Award of the National Scientific and Technological Progress (No.1) in 2011.

Figures

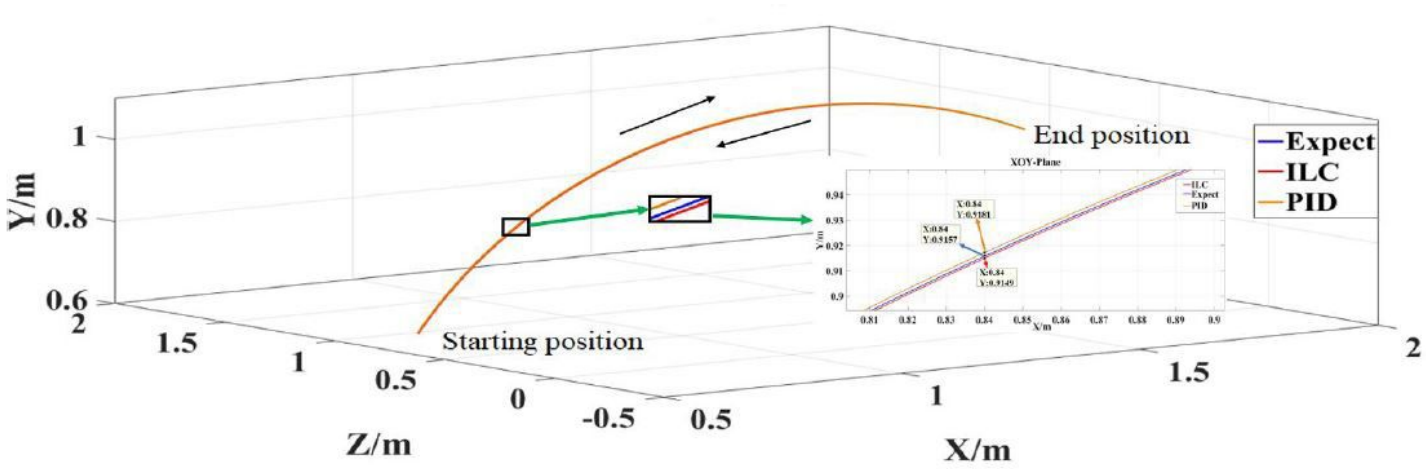

Figure 1

Three-dimensional trajectory tracking test data of PID and PD-type ILC in 20th iteration.

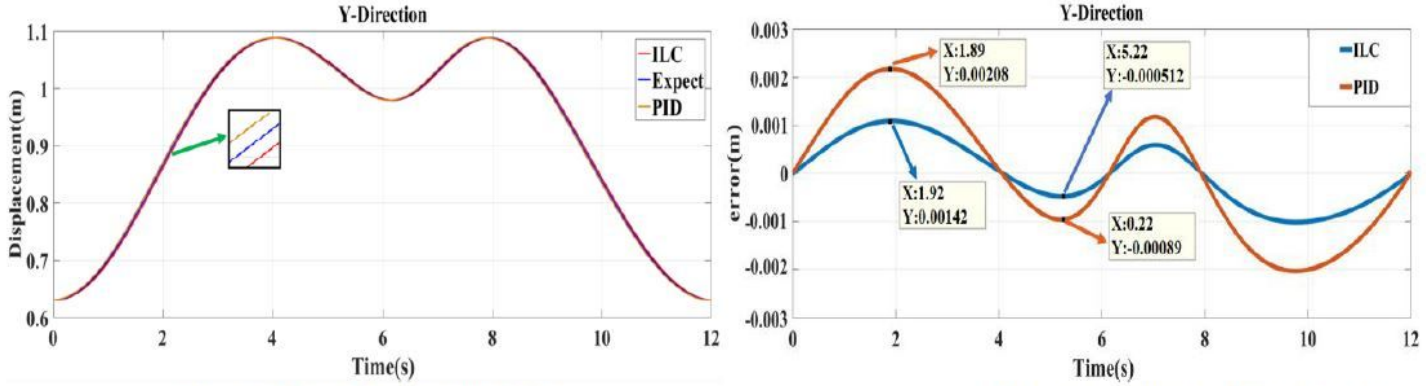

(a) Y axis position tracking curve (b) Y axis position tracking error curve

Figure 2

Y axis test data of PID and PD-type ILC in 20th iteration.

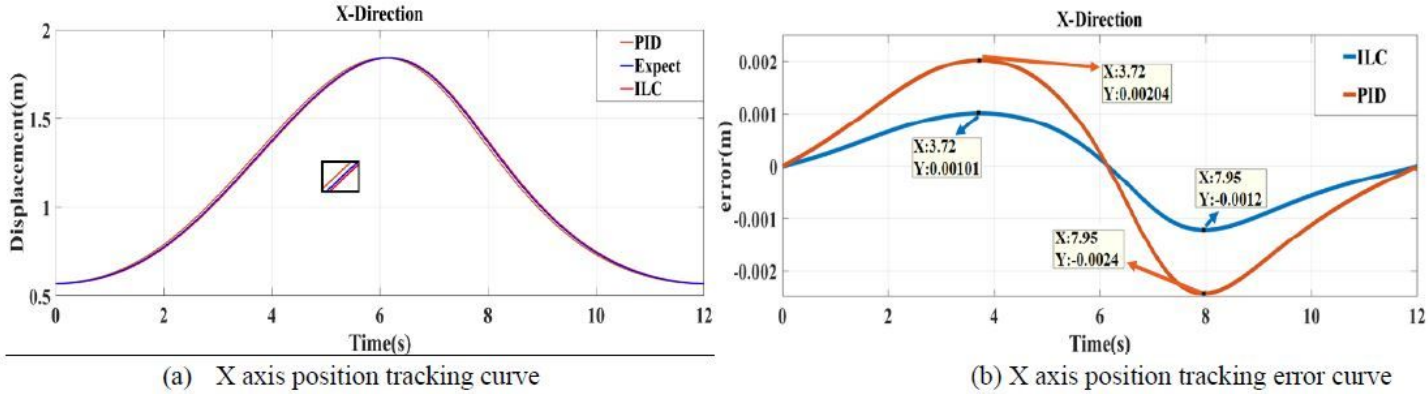

(a) X axis position tracking curve (b) X axis position tracking error curve

Figure 3

X axis test data of PID and PD-type ILC in 20th iteration.

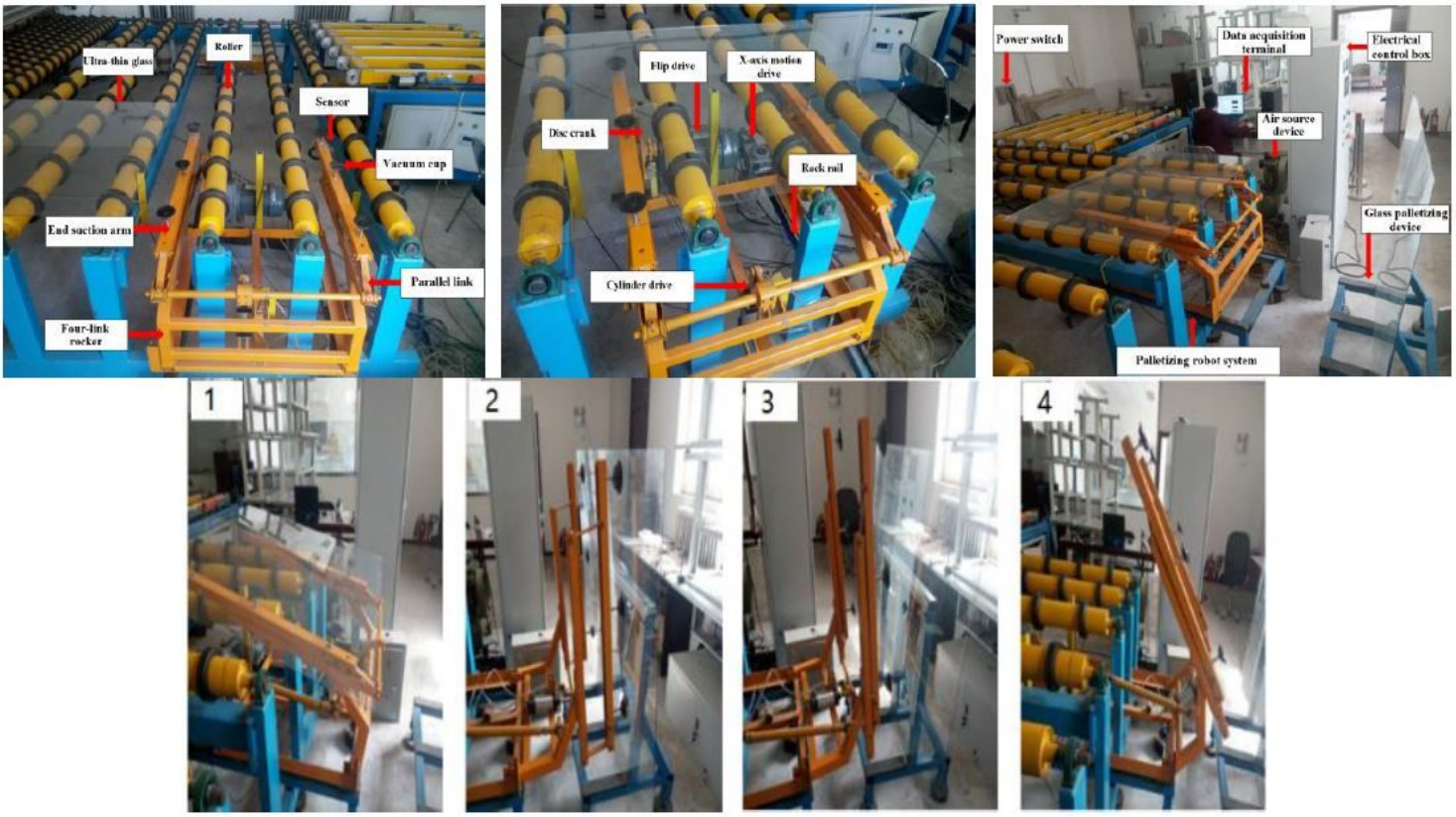

Figure 4

Glass palletizing robot test experiment with multi-link mechanism.

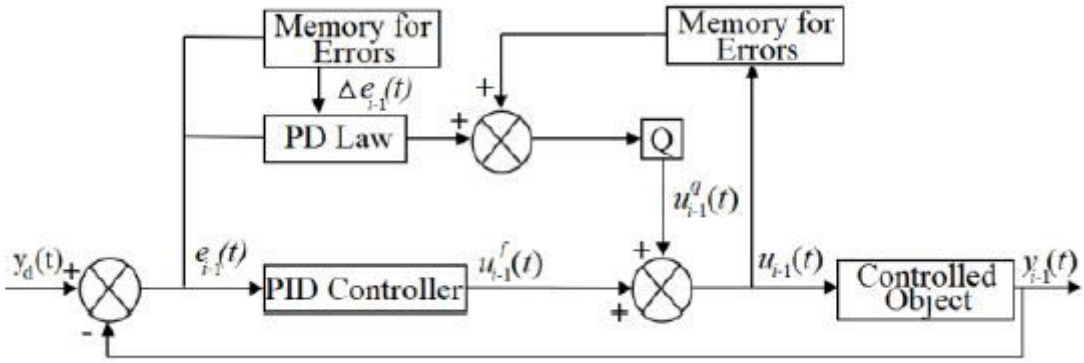

Figure 5

Feedforward-feedback iterative learning control block diagram.

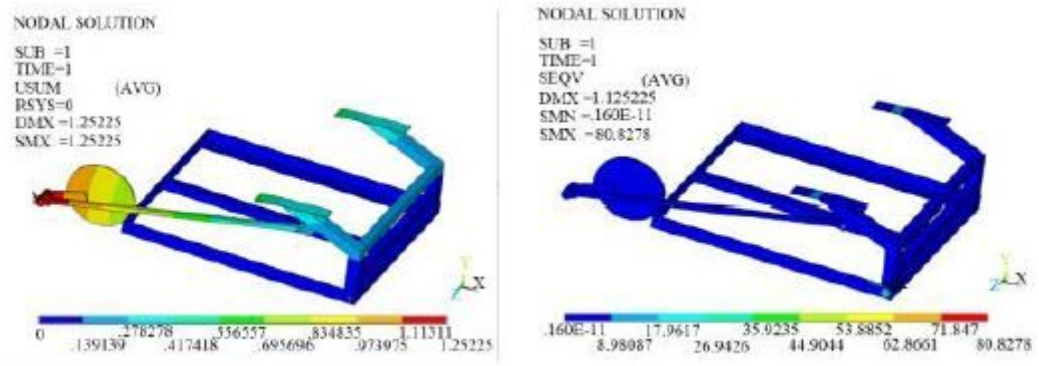

Figure 6

Static analysis cloud diagram of the crank rocker arm

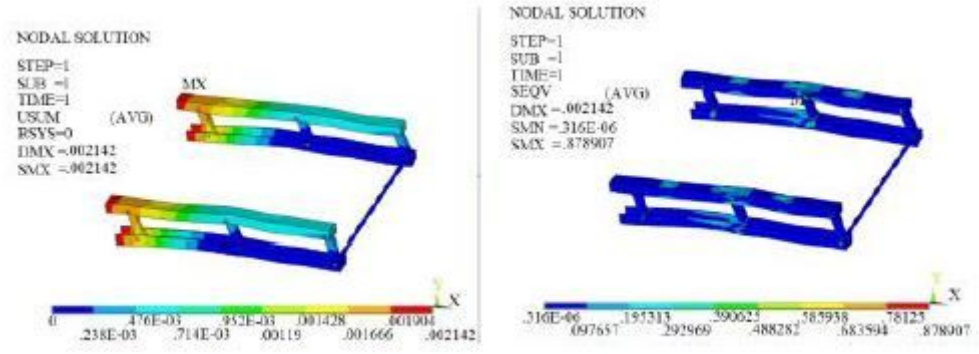

Figure 7

Static analysis cloud diagram of sucker arm

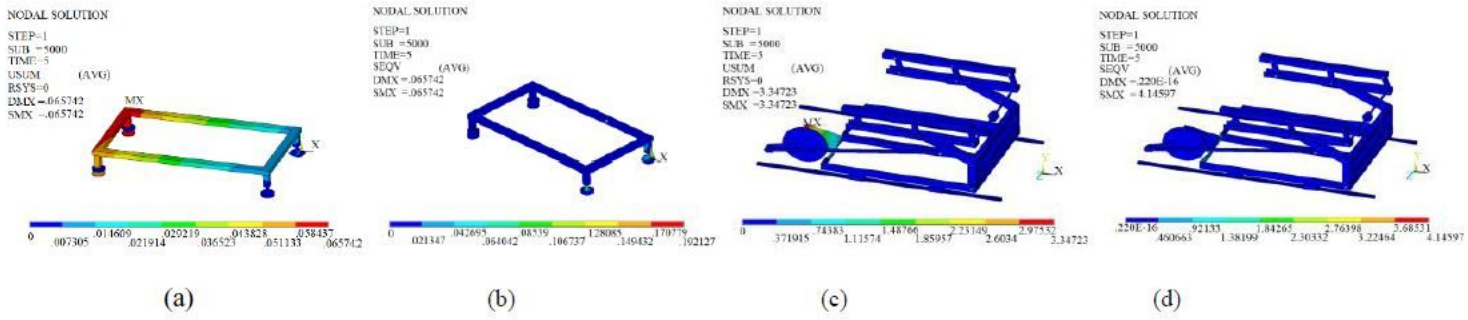

Figure 8

Transient deformation cloud diagram and stress cloud diagram of base support frame and overall rack.

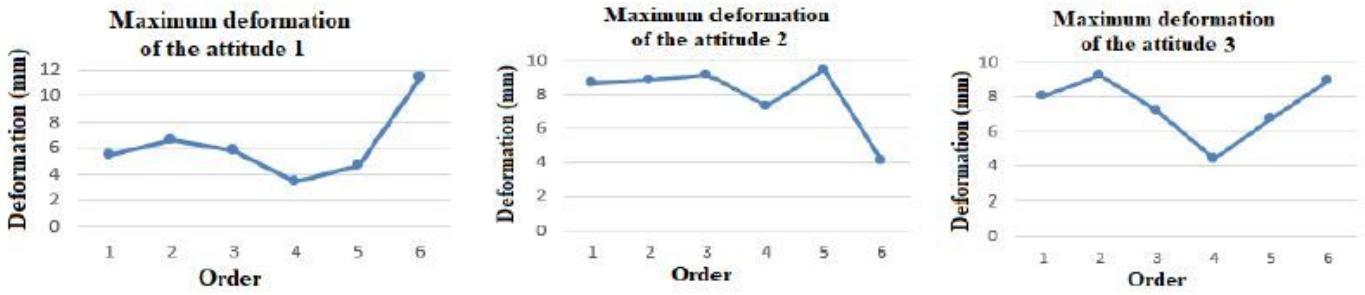

Figure 9

The first-six orders of maximum deformation under the three poses of the manipulator.

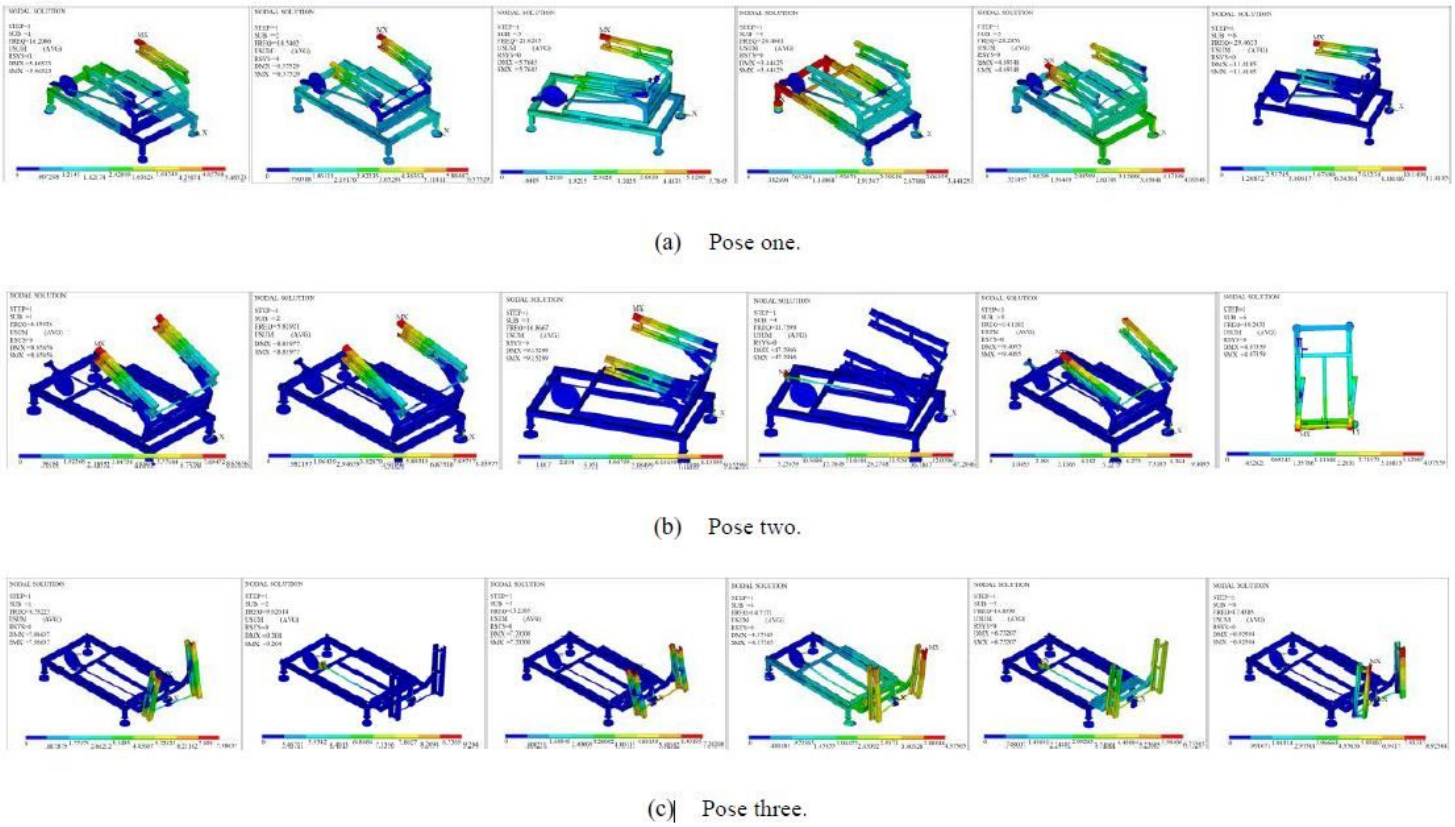

(a) Pose one.

(b) Pose two.

(c) Pose three.

Figure 10

The first-six vibration modes of the robot in three poses.

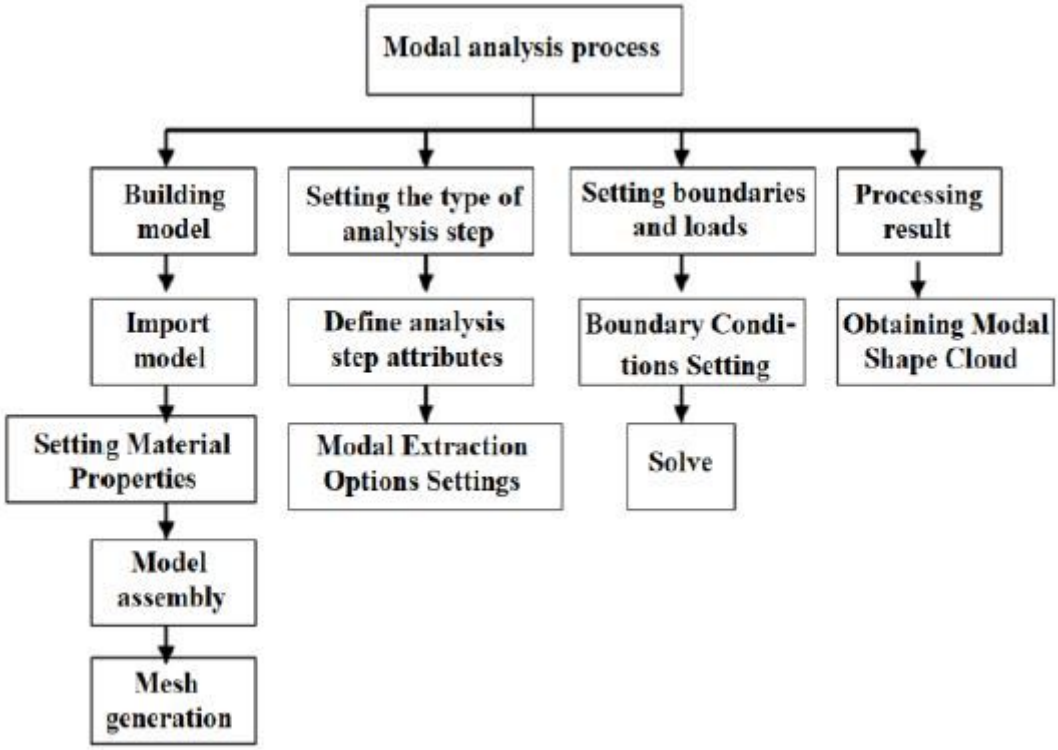

Figure 11

Modal analysis process.

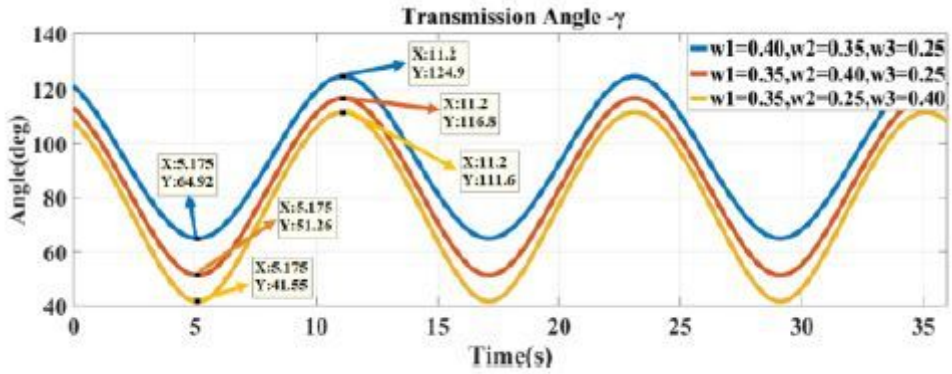

Figure 12

Transmission angle under Three Working Conditions.

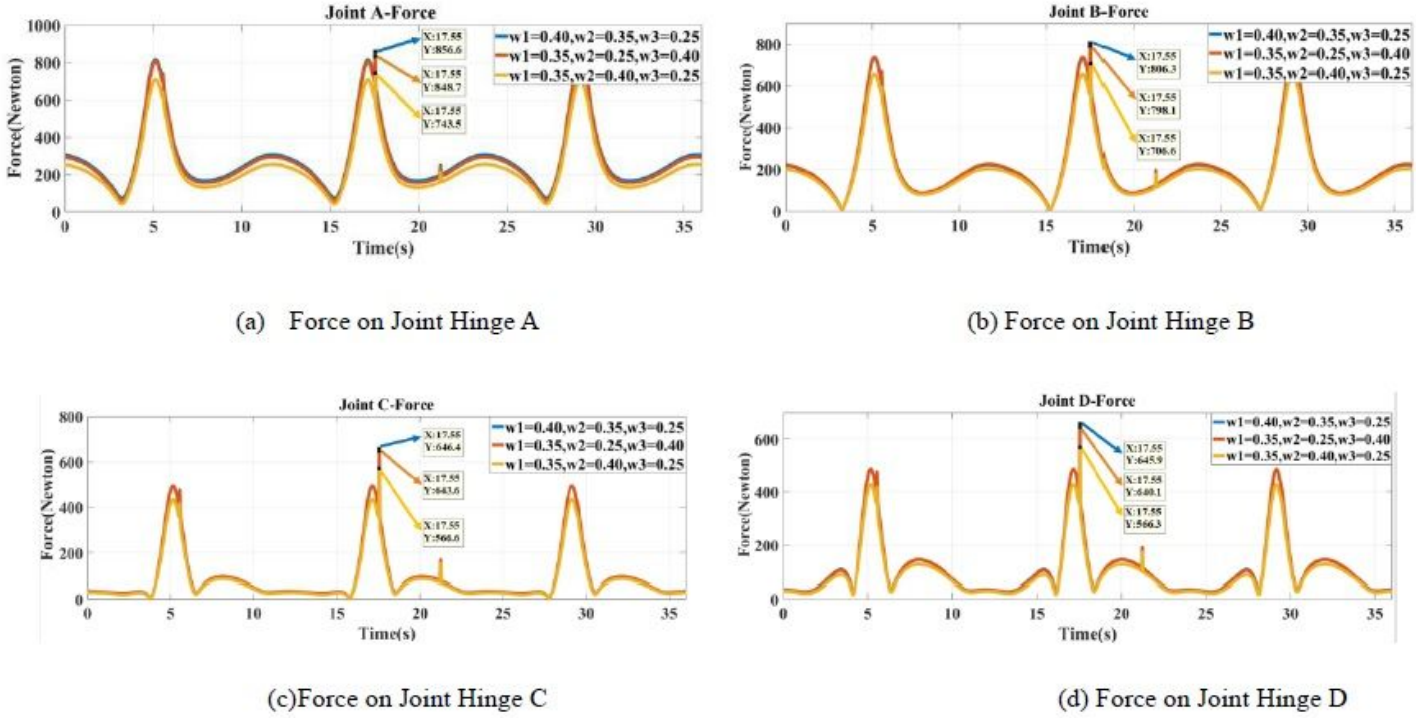

(a) Force on Joint Hinge A

(b) Force on Joint Hinge B

(c)Force on Joint Hinge C

(d) Force on Joint Hinge D

Figure 13

Force on Joint Hinges A, B, C and D under Three Working Conditions.

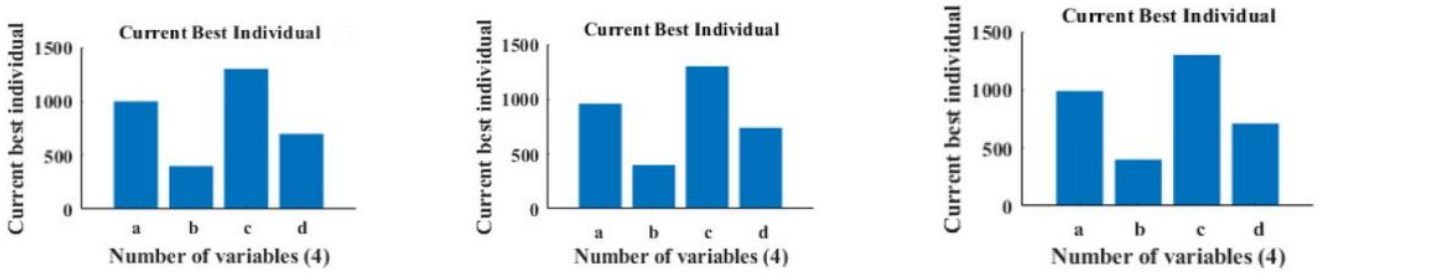

(a) Conditions 1

(b) Conditions 2

(c) Conditions 3

Figure 14

Optimized results under three working conditions.

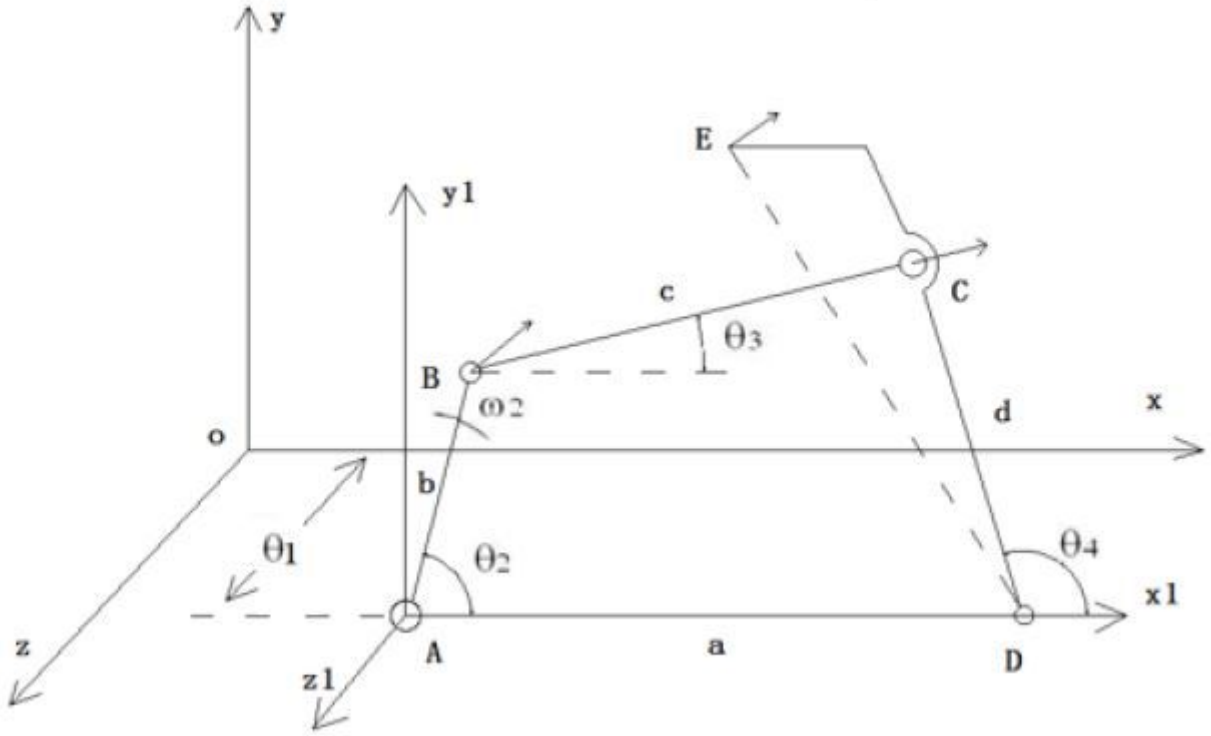

Figure 15

Schematic diagram of the thin plate palletizing robot movement.

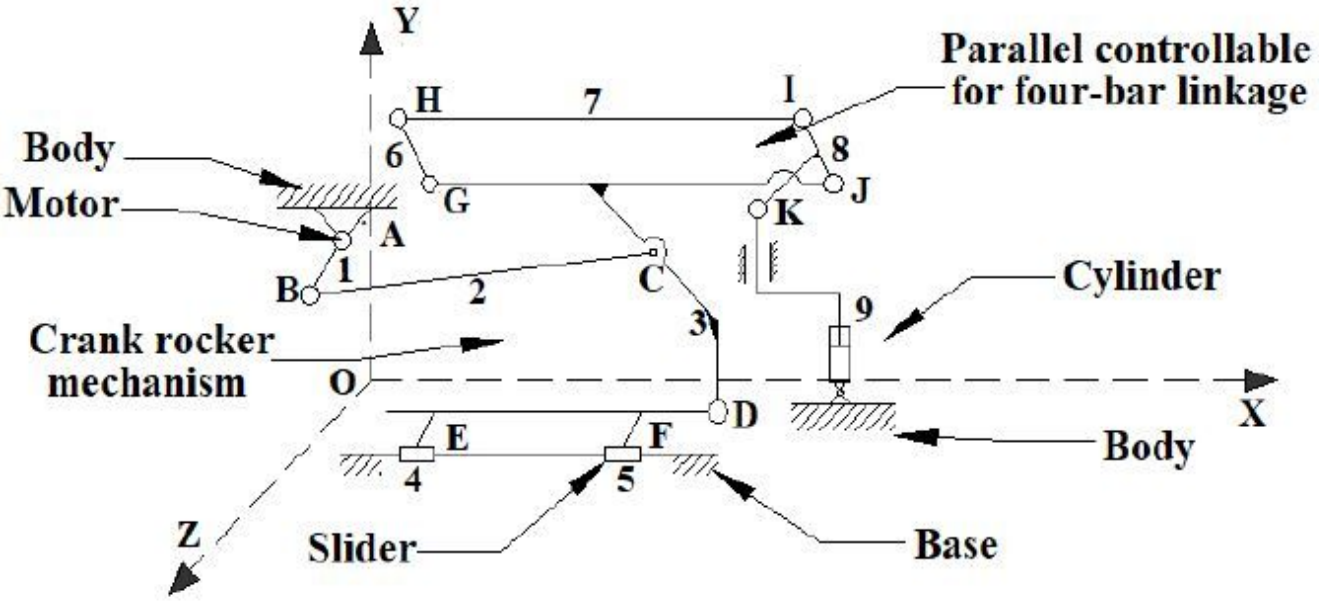

Figure 16

Schematic diagram of the palletizing robot movement.

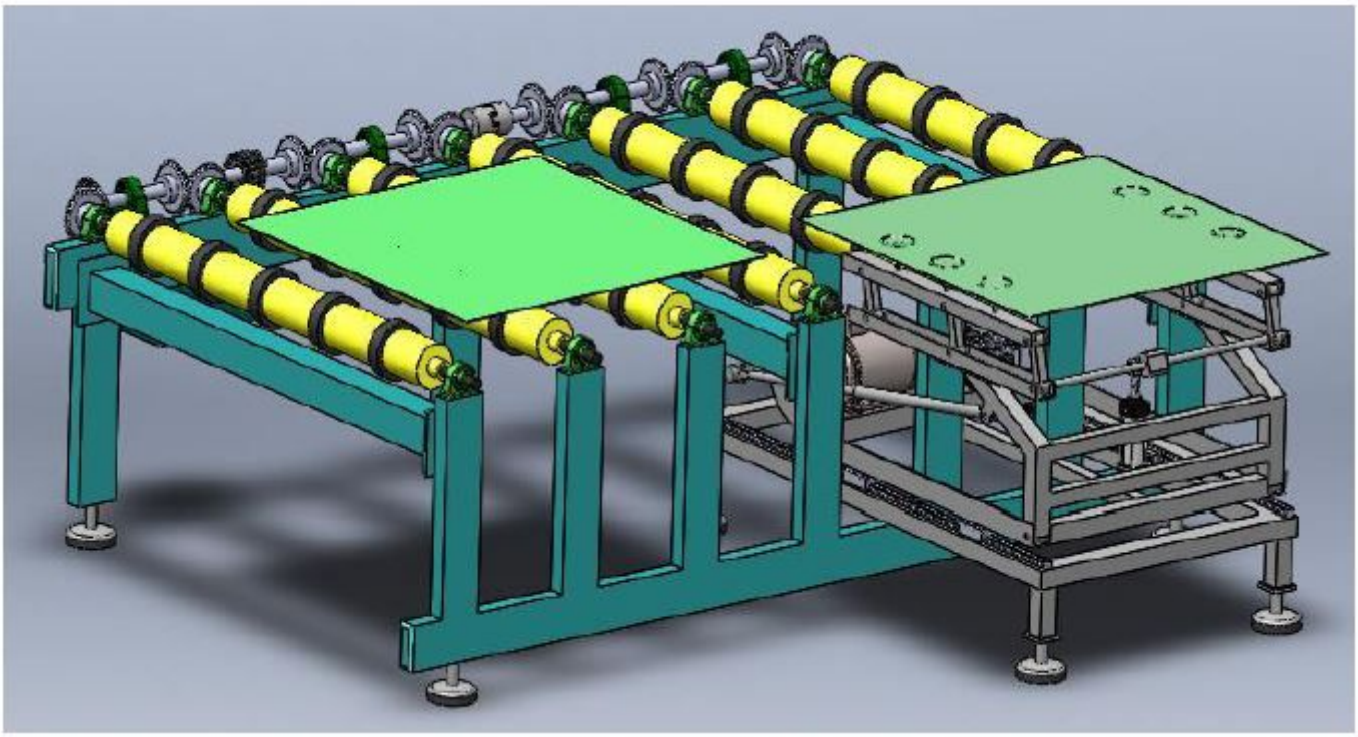

Figure 17

Three-Dimensional Model of Multi-Link Thin Plate Palletizing Robot.

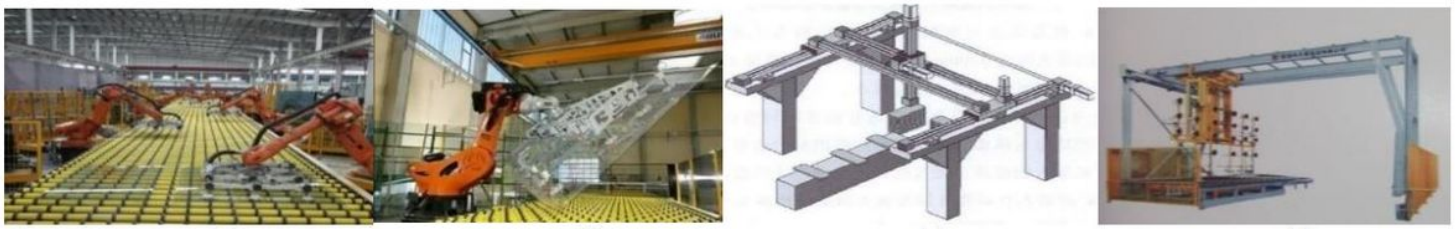

Figure 18

Physical prototype of traditional industrial palletizing manipulator.